THE JOURNAL OF BIOLOGICAL CHEMISTRY VOL. 288, NO. 23, pp. 16460–16475, June 7, 2013

Structure of the Lectin Mannose 6-Phosphate Receptor Homology (MRH) Domain of Glucosidase II, an Enzyme That Regulates Glycoprotein Folding Quality Control in the Endoplasmic Reticulum*

Received for publication, January 3, 2013, and in revised form, April 5, 2013 Published, JBC Papers in Press, April 22, 2013, DOI 10.1074/jbc.M113.450239

Linda J. Olson[‡], Ramiro Orsi[§], Solana G. Alculumbre[§], Francis C. Peterson[‡], Ivan D. Stigliano[§], Armando J. Parodi[§], Cecilia D'Alessio[§¶1], and Nancy M. Dahms[‡2]

From the [‡]Department of Biochemistry, Medical College of Wisconsin, Milwaukee, Wisconsin 53226, [§]Fundación Instituto Leloir and Instituto de Investigaciones Bioquímicas de Buenos Aires, Consejo Nacional de Investigaciones Científicas y Técnicas, C1405BWE Buenos Aires, Argentina, and [¶]School of Sciences, University of Buenos Aires, C1428EHA Buenos Aires, Argentina

Background: Glucosidase II is an endoplasmic reticulum enzyme involved in quality control of glycoprotein folding.
Results: The structure of the lectin domain of GII was determined by NMR spectroscopy.
Conclusion: GII lectin domain structure contains a unique Trp residue critical for GII activity.
Significance: GIIβ MRH domain structure is the first determined of an MRH domain present in a protein with enzymatic activity.

Here we report for the first time the three-dimensional structure of a mannose 6-phosphate receptor homology (MRH) domain present in a protein with enzymatic activity, glucosidase II (GII). GII is involved in glycoprotein folding in the endoplasmic reticulum. GII removes the two innermost glucose residues from the $Glc_3Man_9GlcNAc_2$ transferred to nascent proteins and the glucose added by UDP-Glc:glycoprotein glucosyltransferase. GII is composed of a catalytic GIIα subunit and a regulatory GIIβ subunit. GIIβ participates in the endoplasmic reticulum localization of GIIα and mediates *in vivo* enhancement of *N*-glycan trimming by GII through its C-terminal MRH domain. We determined the structure of a functional GIIβ MRH domain by NMR spectroscopy. It adopts a β-barrel fold similar to that of other MRH domains, but its binding pocket is the most shallow known to date as it accommodates a single mannose residue. In addition, we identified a conserved residue outside the binding pocket (Trp-409) present in GIIβ but not in other MRHs that influences GII glucose trimming activity.

Mannose 6-phosphate receptor homology (MRH)[3] domains were first described in the two receptors responsible for delivering lysosomal enzymes from the *trans* Golgi network to endosomal compartments in mammalian cells. In these mannose 6-phosphate receptors (MPRs), the MRH domains require the presence of mannose-linked phosphate groups in *N*-glycans for binding, a structural feature not required by MRH domains present in other proteins of the secretory pathway (1). Of the known MRH domain-containing proteins, three are endoplasmic reticulum (ER)-resident proteins, OS-9 (Yos9p is the yeast homolog of mammalian OS-9), Erlectin (also called XTP3-B), and glucosidase II (GII) (2).

A quality control mechanism reliant on *N*-glycan structures exists in the ER and ensures the correct folding of glycoproteins within the secretory pathway of eukaryotic cells (see Fig. 1*A*) (3, 4). OS-9 and Erlectin are apparently involved in driving misfolded glycoproteins to proteasomal degradation. The *N*-glycan structural requirements for OS-9/Yos9p binding have been studied in detail. Optimal recognition occurs in glycans lacking residues *i* and *k* (see Fig. 1*B*), thus exposing an α(1,6)-linked mannose unit (residue *j*) (5–7). ER mannose removal (first residue *i* followed by *k*) from the transferred glycan ($Glc_3Man_9GlcNAc_2$) is a relatively slow process compared with deglucosylation and thus occurs mainly in slow folding/misfolded glycoproteins. Thus, the *N*-glycan binding specificity of OS-9/Yos9p is particularly suited for the known function of this protein. The binding specificity of the C-terminal MRH domain of Erlectin for Man_9 has recently been reported, and it was

* This work was supported, in whole or in part, by National Institutes of Health Grants R01DK042667 (to N. M. D.) and GM44500 (to A. J. P.). This work was also supported by Mizutani Foundation for Glycoscience Grant 10-0056 (to N. M. D.), Agencia Nacional de Promoción Científica y Tecnológica Grant PICT 2010-0734 and the Howard Hughes Medical Institute (to A. P.), and *Consejo Nacional de Investigaciones Científicas y Técnicas* Grant PIP-N824 and *University of Buenos Aires* Grant UBACYT-X290 (to C. D.).
The GIIβ MRH domain structure has been deposited in the Biological Magnetic Resonance Data Bank under BMRB accession number 18592.
The atomic coordinates and structure factors (code 2LVX) have been deposited in the Protein Data Bank (http://wwpdb.org/).
[1] To whom correspondence may be addressed: Laboratory of Glycobiology, Fundación Inst. Leloir-Inst. de Investigaciones Bioquímicas de Buenos Aires-CONICET, Av. Patricias Argentinas 435, C1405BWE Buenos Aires, Argentina and School of Sciences, University of Buenos Aires, C1428EHA Buenos Aires, Argentina. Tel.: 5411-5238-7500 (ext. 2302); Fax: 5411-5238-7501; E-mail: cdalessio@leloir.org.ar.
[2] To whom correspondence may be addressed: Dept. of Biochemistry, Medical College of Wisconsin, 8701 Watertown Plank Rd., Milwaukee, WI 53226. Tel.: 414-955-4698; Fax: 414-955-6510; E-mail: ndahms@mcw.edu.

[3] The abbreviations used are: MRH, mannose 6-phosphate receptor homology; MPR, mannose 6-phosphate receptor; ER, endoplasmic reticulum; GII, glucosidase II; pNPG, *p*-nitrophenyl α-D-glucopyranoside; SPR, surface plasmon resonance; GAA, acid α-glucosidase; CI-MPR, cation-independent MPR; CD-MPR, cation-dependent MPR; Man-6-P, mannose 6-phosphate; Glc-6-P, glucose 6-phosphate; SUMO, small ubiquitin-like modifier; HSQC, heteronuclear single quantum coherence; r.m.s.d., root mean square deviation; UGGT, UDP-Glc:glycoprotein glucosyltransferase.

proposed to serve as a negative regulator of ER-associated degradation (8). In contrast to these two proteins, GII is an early player in *N*-glycan processing as it removes the two inner glucoses from all transferred glycans (residues *l* and *m*; see Fig. 1*B*) irrespective of the folding status of the protein. Removal of the middle glucose (residue *m*) creates a monoglucosylated epitope that is recognized by two unconventional chaperones, the lectins calnexin and calreticulin. Their interactions with glycoproteins enhance the folding efficiency of nascent polypeptides and prevent the exit of folding intermediates and misfolded glycoproteins from the Golgi. Monoglucosylated *N*-glycans may be also formed by the action of UDP-Glc:glycoprotein glucosyltransferase (UGGT) on fully deglucosylated glycans linked to protein moieties not displaying their native structures (see Fig. 1*A*).

GII is a heterodimer composed of a catalytic GIIα subunit and a regulatory GIIβ subunit that contains an MRH domain and in most species a KDEL-like ER retrieval sequence at its C terminus (9, 10) (see Fig. 2*A*). Contrary to OS-9/Yos9p, maximal *N*-glycan binding by GIIβ MRH domain requires the presence of mannose residue *k* of arm C (Fig. 1*B*). Furthermore, *in vivo* and cell free assays show that a decrease in *N*-glycan mannose content results in lower GII enzymatic activity (11–15). Not only does optimal GII deglucosylation activity require the presence of the full complement of mannose units on nascent glycoproteins but also the four conserved amino acids of the GIIβ subunit that are known to be essential for the ability of the MRH domains of MPRs to bind mannose 6-phosphate (Man-6-P)-containing lysosomal enzymes (15, 16) (Fig. 2*B*).

Why does GII differ from most other glycosidases for which their maximal activity does not require the presence of a lectin-like domain? We have shown previously that a decrease in *N*-glycan mannose content sharply decreases *in vivo* GII activity without affecting the activity of UGGT, thereby prolonging the half-life of monoglucosylated glycans produced by UGGT (15). We speculate that ER mannosidase-mediated removal of mannose units would result in an increased interaction of slow folding/misfolded glycoproteins with the lectin chaperones. This in turn would increase the chances for proper folding of glycoproteins displaying an arduous folding process and would result in a more stringent prevention of a surreptitious exit of misfolded glycoproteins to the Golgi. Therefore, the presence of the MRH domain converts GII into a key regulator of the quality control mechanism of glycoprotein folding. As the structure of OS-9 MRH domain was recently determined (7), the significant difference between its *N*-glycan binding specificity and that of GII prompted us to determine the structure of GIIβ MRH domain. Here we report that GIIβ MRH domain folds into a flattened β-barrel similar to that of the MPRs and OS-9, but its binding pocket is the most shallow solved to date. Moreover, we identified a residue (Trp-409) important for GII activity and propose two models of how it could be influencing GIIβ-mediated enhancement of GII activity.

EXPERIMENTAL PROCEDURES

Materials—Yeast extract and Bacto Peptone were from Difco. Endo-β-*N*-acetylglucosaminidase H, porcine trypsin, protease inhibitors, *p*-nitrophenyl α-D-glucopyranoside (pNPG), dithiothreitol (DTT), [^{15}N]ammonium chloride, [^{13}C]glucose, Man-6-P, amino acids and supplements for culture media, and protease inhibitors were from Sigma. [^{14}C]Glucose (301 Ci/mol) was from PerkinElmer Life Sciences. *N*-Methyl-1-deoxynojirimycin was from Toronto Biochemicals. Manα1,2Man was obtained from Dextra Laboratories (UK).

Strains and Media—Escherichia coli DH5α was used for cloning purposes. Recombinant GIIβ expression was performed in SHuffle T7 Express *lysY* competent *E. coli* cells (BL21 C3030, New England Biolabs). Bacteria were grown at 37 °C in LB medium (0.5% NaCl, 1% tryptone, 0.5% yeast extract) supplemented with 200 μg/ml ampicillin or 50 μg/ml kanamycin as needed. *Schizosaccharomyces pombe* cells were grown at 28 °C in rich YES medium (0.5% yeast extract, 3% glucose, and 75 μg/liter adenine) or Edinburgh minimal medium (17, 18) supplemented with adenine (75 μg/liter), uracil (75 μg/liter), and/or leucine (250 μg/liter) for selective growth. Thiamine (0.5 μM) was added to pREP3x-GIIαVDEL-transformed strains to control expression levels from *nmt1* promoter. *S. pombe* strains used were Sp61IIα (Δ*GIIα*: *h*$^-$, *leu1–32*, *ade6-M210*, *ade1*, *ura4-D18*, Δ*gls2α*::*ura4*$^+$), ADmIIβ (Δ*GIIβ*: *h*$^-$, *leu1–32*, *ade6-M210*, *ura4-D18*, Δ*gls2β*::*ura4*$^+$), and SpADIIαβ (Δ*GIIαβ*: *h*$^-$, *leu1–32*, *ade6-M216*, *ura4-D18* Δ*gls2α*::*ura4*$^+$, Δ*gls2β*::*ura4*$^+$) as described (14).

Cloning and Expression of Recombinant Mature S. pombe GIIβ—Total RNA from *S. pombe* was obtained from exponentially growing *S. pombe* wild-type cultures as described (19). GIIβ-coding DNA lacking the signal peptide (first 23 amino acids) sequence was obtained by RT-PCR using the primers B2sNde1 (5′-GGAATTCCATATGGCAAATGACCTCCGTGGTG-3′) and B2aNot1 (5′-ATAGTTTAGCGGCCGCCTCATCGACAGATGATTC-3′) that include NdeI and NotI restriction sites (underlined) and a Superscript II reverse transcriptase kit (Invitrogen). The PCR product was cloned in NdeI/NotI sites of pET22b(+) vector as a C-terminal His_6 fusion protein. The construction was transformed into BL21 3030 cells. After an overnight induction at 18 °C with 1.5 mM isopropyl β-D-thiogalactoside, bacteria were lysed by sonification in binding buffer (20 mM Tris-HCl, pH 7.9, 0.5 mM NaCl, 5 mM imidazole) with 0.5% (v/v) Triton X-100, 1 mg/ml lysozyme, and protease inhibitors (100 μM PMSF, 10 μM leupeptin, 10 μM pepstatin, and 10 μM E64) and centrifuged for 20 min at 20,000 × *g*. The protein was purified from the supernatant by immobilized metal ion affinity chromatography using a column loaded with chelating Sepharose (GE Healthcare) precharged with $NiCl_2$. After extensive washes with binding buffer followed with wash buffer (binding buffer plus 60 mM imidazole), elution was performed with elution buffer (binding buffer plus 1 M imidazole). The protein was dialyzed against 50 mM phosphate buffer, pH 7.4, 100 mM NaCl. The purification and identity of the protein in the soluble fraction were verified by 10% SDS-polyacrylamide gel electrophoresis (PAGE) and Western blot, respectively, with a mouse polyclonal anti-GIIβ *S. pombe* antibody (1:1000; Ref. 14) and mouse anti-His (1:1000; Sigma).

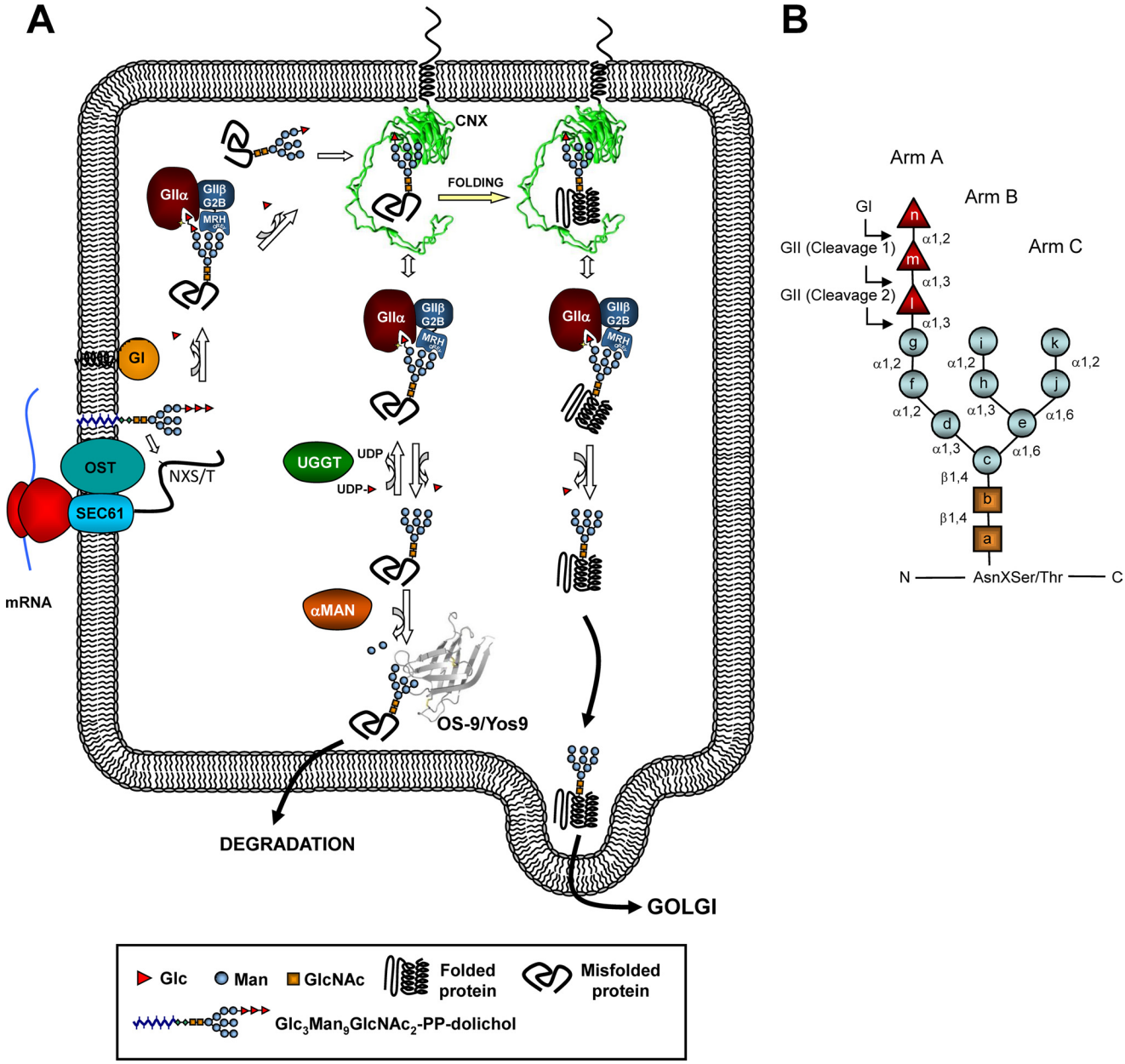

FIGURE 1. **Quality control of glycoprotein folding in the ER.** *A*, schematic diagram of the glycan-processing steps during quality control of glycoprotein folding in the ER. During *N*-glycosylation, a glycan ($Glc_3Man_9GlcNAc_2$; *B*) is transferred to the Asn-*X*-Ser/Thr sequence of nascent proteins that are being translocated into the ER. The sequential action of glucosidase I (*GI*) and GII produces monoglucosylated glycans able to interact with the lectin chaperones calnexin (*CNX*) and/or calreticulin (*CRT*). This interaction facilitates both glycoprotein folding and interaction with the protein-disulfide isomerase ERp57, thus preventing exit from the ER of misfolded glycoproteins until proper folding is achieved (4, 45). The formation of monoglucosylated glycoproteins occurs either by deglucosylation of the transferred *N*-glycan or by reglucosylation by UGGT. UGGT is a glycoprotein folding status sensor that transfers a glucose residue to the $Man_9GlcNAc_2$ oligosaccharide of glycoproteins that have not yet acquired their native structure. Removal of mannose residues by α-mannosidase(s) generates a degradation signal on misfolded/slow folding glycoproteins. OS-9 recognizes Manα1,6Manα1,6Man on the trimmed C arm via its MRH domain (7) and facilitates entry of misfolded glycoproteins into the ER-associated degradation pathway where the misfolded glycoproteins exit the ER and are degraded by the proteasome in the cytosol. *SEC61*, translocon; *OST*, oligosaccharyltransferase; ribbon diagram representing the crystal structure of calnexin is shown (Protein Data Bank code 1JHN (53)); *α-MAN*, α-mannosidase; ribbon diagram of human OS-9 is shown (Protein Data Bank code 3AIH (7)). *B*, structure of the oligosaccharide transferred to proteins during *N*-glycosylation. *Lettering* (*a–n*) follows the order of monosaccharide addition during the synthesis of $Glc_3Man_9GlcNAc_2$-P-P-dolichol. Glucosidase I (*GI*) removes residue *n*. GII removes residues *l* and *m*. UGGT adds residue *l* to residue *g*.

S. pombe Microsomal Fraction Preparations—*S. pombe* microsomes were prepared from 250 ml of exponentially growing cultures at an A_{600} of 2. Cells were harvested, washed with 5 mM NaN_3, and broken by 10 repetitive cycles of 1-min vortexing on ice with glass beads in 0.25 M sucrose, 20 mM imidazole, 5 mM EDTA with protease inhibitors (100 μM PMSF, 10 μM L-1-tosylamido-2-phenylethyl chloromethyl ketone, 10 μM *N-p*-tosyl-L-lysine chloromethyl ketone, 10 μM leupeptin, 10 μM pepstatin, and 10 μM E64), and the microsomal fraction was obtained as described (10). Protein concentrations were determined using a Bio-Rad protein assay as described by the manufacturer.

Protein Expression and Purification of S. pombe GIIβ MRH Domain—MRH GIIβ cDNA encoding residues 357–450 was cloned into a pQE30 vector modified to express the small ubiq-

uitin-like modifier (SUMO) protein with an N-terminal hexa-His tag and transformed into BL21(pREP4) cells. Constructs containing the amino acid substitutions W409A and W409F were generated using the QuikChange® Lightning site-directed mutagenesis kit (Stratagene). Cells were grown at 37 °C until an OD of ~0.7 at which time protein expression was induced by the addition of 1 mM isopropyl β-D-thiogalactoside. Cells were harvested after 18 h. Protein was purified from insoluble inclusion bodies using metal affinity chromatography. Refolding was performed by diluting the protein into 100 mM Tris, pH 8.0, 10 mM cysteine, 0.5 mM cystine and stirring for 2 h at 22 °C. Following concentration, the SUMO-specific peptidase ULP-1 was added to remove the SUMO domain. The protein was dialyzed and subjected to metal affinity chromatography to separate the cleaved SUMO peptide from the MRH domain. Protein for NMR analyses was then buffer-exchanged into a solution containing 10 mM deuterated imidazole (pH 7.1) and 150 mM NaCl. The protein was further purified by size exclusion chromatography using a Superdex 75 column. The concentration of the purified protein was determined using the Bradford assay (Bio-Rad) with bovine serum albumin (BSA) as the standard.

GIIβ Mutagenesis and Expression in S. pombe—The Gateway pDONR201 plasmid containing clone 26/D11 (*S. pombe* GIIβ subunit, which was obtained from RIKEN DNA Bank (20)) was used as the template for single amino acid PCR mutagenesis of the GIIβ MRH domain (W409A or W409F). The amplified mutant DNA containing both GIIβ and vector sequences was phosphorylated, religated, and electroporated into DH5α cells. The following primers were used (mutagenic codons are underlined): W409F forward mutagenic primer 5′-TTCAATGGTCCTCATAGATCTGCC-3′ or W409A forward mutagenic primer 5′-GCTAATGGTCCTCATAGATCTGCC-3′ was used with W409 reverse primer 5′-GCAACTTTGACCATTTTCATAC-3′. Wild-type and mutant GIIβ DNA clones were transferred to the pREP1-ccdb2 Gateway-compatible *S. pombe* destination expression vector (RIKEN DNA Bank) by the LR recombination reaction (Invitrogen). *S. pombe* competent Δ*GIIβ* cells were electroporated with the pREP1-GIIβ episomal constructs. The MRH binding pocket mutant constructs used in this study (pREP1-GIIβ Y462F and pREP1-GIIβ E456Q) were described in Stigliano *et al.* (14). Please note that the numbering in that case starts with the initial methionine, although throughout this work the numbering corresponds to the mature protein sequence.

Synthesis of Labeled N-Glycan Substrates—[^{14}C-Glc]-$Glc_1Man_9GlcNAc$ was obtained by glucosylation of denatured bovine thyroglobulin in the presence of UDP-[^{14}C]glucose (obtained as described (21)) and rat liver microsomes followed by purification of endoglycosidase H-sensitive *N*-glycans as described previously (22). Monoglucosylated glycans were separated from the unglucosylated compounds by two successive paper chromatographic separations performed in 1-propanol/nitromethane/H_2O (5:2:4).

GII Activity Assays—GII activities using the small substrate analog pNPG and labeled *N*-glycans as substrates were assayed in *S. pombe* microsomal fractions as described (14). Briefly GII activity in Δ*GIIβ* mutants transformed with wild-type or mutant regulatory subunits was assayed using 5 mM pNPG as the substrate in 0.1 M HEPES buffer, pH 7.2 for 20 min at 37 °C, and absorbance at 405 nm was measured, or [^{14}C-Glc]$Glc_1Man_9GlcNAc$ was used as the substrate in 40 mM sodium phosphate buffer, pH 7.2 for 15 min at 30 °C. In the latter case, glucosidase activity was determined as the percentage of total glucose released. Complementation assays between GIIα and endogenous GIIβ were performed using a mixture of 125 μg of proteins from microsomes containing GIIα but not GIIβ (Δ*GIIαβ* cells transformed with pREP3x-GIIαVDEL as described (14)) with 125 μg of proteins from microsomes containing GIIβ but not GIIα (Δ*GIIα S. pombe* cells expressing only endogenous GIIβ). When assaying GIIβ enhancement of GIIα activity toward *N*-glycans of recombinant GIIβ or MRH, the microsomal source of GIIβ subunit was replaced with 125 ng of pure recombinant GIIβ (this is in the linear range of activation; data not shown) or with the indicated MRH/GIIβ or BSA/GIIβ mass ratios. The mixtures were preincubated for 30 min at 4 °C in the presence of 1% Triton X-100 and then assayed for GII activity with [^{14}C-Glc]$Glc_1Man_9GlcNAc$ as described above.

Purification of $Man_9GlcNAc$—$Man_9GlcNAc$ was obtained from endo-β-*N*-acetylglucosaminidase H-digested denatured soybean agglutinin purified from untoasted soybean meal by affinity chromatography on acid-treated Sepharose 6B (23). Soybean agglutinin (10 mg) was denatured in 8 M urea for 5 h at 65 °C; dialyzed against H_2O; preincubated for 10 min at 95 °C in 0.5% SDS, 0.1 M β-mercaptoethanol in 50 mM triethylamine acetate buffer, pH 5.5; and treated with 20 milliunits of endo-β-*N*-acetylglucosaminidase H (Sigma) for 16 h at 37 °C. Proteins were precipitated with 66% methanol. To separate Man_9 from remaining proteins, the supernatant was dried, resuspended in 10% ethanol, and resolved in a Superdex Peptide gel filtration column (GE Healthcare) in 10% ethanol at 1 ml/min. The glycan-containing fractions were detected using the phenol-sulfuric acid assay (24), and protein elution was monitored by absorbance at 280 nm.

Analysis of Glycans Synthesized in Vivo—To assess ER *N*-glycan composition, *S. pombe* cells in the exponential growth phase expressing GIIβ mutations were harvested, extensively washed with 1% yeast nitrogen base medium without glucose, and resuspended in 2 volumes (v/w) of the same medium. Cells (0.5 ml) were then preincubated for 5 min in 5 mM DTT and pulsed for 15 min with 5 mM glucose containing 150 μCi of [^{14}C]glucose (300 Ci/mol). Further details on the labeling procedure and the preparation of whole cell endo-β-*N*-acetylglucosaminidase H-sensitive *N*-glycans have been described previously (25). Glycans were separated by paper chromatography using Whatman 1 papers and 1-propanol/nitromethane/H_2O (5:2:4) as solvent, and the peaks were identified by standards run in parallel. To improve the resolution, the identified glycans were eluted from paper and resolved by HPLC using a TSKgel Amide-80 column (4.6-mm inner diameter × 25 cm; Tosoh) with a mobile phase of H_2O/CH_3CN in a linear gradient from 35:65 to 55:45 over 65 min and a flow rate of 0.75 ml/min at room temperature. Because of slight variations in retention times among runs, the positions of the peaks in paper chromatography and not the retention times from HPLC were used to identify glycans.

Surface Plasmon Resonance (SPR) Analyses—Biosensor studies were carried out as described previously (26). All SPR measurements were performed at 25 °C using a BIAcore 3000 instrument (GE Healthcare). Purified protein (acid α-glucosidase (GAA), GAA phosphomonoester, or GAA phosphodiester) was immobilized on a CM5 sensor chip (GE Healthcare) following activation of the surface using 1-ethyl-3-(3-dimethylaminopropyl)carbodiimide and *N*-hydroxysuccinimide. The proteins were injected onto the activated dextran surface at a concentration of 10–20 μg/ml in 10 mM sodium acetate buffer, pH 5.0 (GAA phosphomonoester), pH 4.5 (GAA phosphodiester), or pH 5.0 (GAA) using immobilization buffer (10 mM MES, pH 6.5, 150 mM NaCl, 0.005% (v/v) P20) as the running buffer. After coupling, unreacted *N*-hydroxysuccinimide ester groups were blocked with ethanolamine. The reference surface was treated in the same way except that protein was omitted. To assess binding affinities, samples of purified proteins were prepared in running buffer (50 mM imidazole, pH 7.4, 150 mM NaCl) and injected in a volume of 80 μl over the coupled and reference flow cells at a flow rate of 40 μl/min. After 2 min, the solutions containing the purified proteins were replaced with buffer, and the complexes were allowed to dissociate for 3 min. The sensor chip surface was regenerated with a 10-μl injection of 10 mM HCl at a flow rate of 10 μl/min. The surface was allowed to re-equilibrate in running buffer for 1 min prior to subsequent injections. The response at equilibrium (R_{eq}) for each concentration of protein was determined by averaging the response over a 10-s period within the steady state region of the sensorgram using the BIAevaluation software package (version 4.0.1). The response at equilibrium (R_{eq}) was plotted *versus* the concentration of protein and fitted by nonlinear regression to a one-site saturation binding model using the equation $y = (R_{max} \times [MPR])/(K_d + [MPR])$ (SigmaPlot version 10.0, Systat Software, Inc.). All response data were double referenced (27) where controls for the contribution of the change in refractive index were performed in parallel with flow cells derivatized in the absence of protein and subtracted from all binding sensorgrams.

Data Collection and Structure Determination by Heteronuclear NMR Spectroscopy—NMR spectra were acquired at 25 °C on a Bruker 600-MHz spectrometer equipped with a triple resonance CryoProbe™. Spectral data were processed using NMRPipe (28) and visualized using XEASY (29). Complete ^{1}H, ^{15}N, and ^{13}C resonance assignments for GIIβ MRH domain were obtained in a semiautomated manner using peak lists from three-dimensional HNCO, HNCOCA, HNCOCACB, HNCA, HNCACB, HNCACO, CCONH, HBHACONH, HCCONH, and HCCH total correlation spectroscopy and ^{13}C (aromatic)-edited NOESY-HSQC spectra and the assignment program GARANT (30). Automated assignments were verified and completed by manual inspection. Structures of the GIIβ MRH domain were calculated using distance constraints derived from three-dimensional ^{15}N-edited NOESY-HSQC and ^{13}C-edited NOESY-HSQC spectra (τ_{mix} = 80 ms). Backbone ϕ and ψ dihedral angle constraints were generated using TALOS+ (31) and the secondary shifts of the ^{1}H, $^{13}C\alpha$, $^{13}C\beta$, $^{13}C'$, and ^{15}N nuclei. Initial structures were generated in an automated manner using the NOEASSIGN module of the torsion angle dynamics program CYANA (32). Initial structures underwent iterative rounds of manual refinement in CYANA to eliminate constraint violations. The top 20 CYANA conformers with the lowest target function were further refined using an Xplor-NIH (33) molecular dynamics protocol in explicit solvent (34). The structural statistics are listed in Table 1.

Determination of Binding Affinities by Heteronuclear NMR Spectroscopy—NMR studies in which ^{15}N-labeled GIIβ MRH domain was titrated with increasing concentrations of ligand (Man-6-P (Sigma), Manα1,2Man (Dextra Laboratories), or $Man_9GlcNAc$ purified from soybean agglutinin were carried out as described previously (35).

Antibodies and Immunodetection—Microsomal *S. pombe* proteins (250 μg) were resolved in a 10% SDS-PAGE, electroblotted to ImmobilonP membranes (Millipore), and incubated with mouse anti-*S. pombe* GIIα or mouse anti-*S. pombe* GIIβ antibodies. Immunodetection was carried out using enhanced chemiluminescence (West Pico SuperSignal Chemiluminescent Substrate, Thermo Scientific) with horseradish peroxidase-conjugated IgGs (Sigma) as described (15).

RESULTS AND DISCUSSION

Full Functionality of the E. coli-expressed S. pombe GIIβ MRH Domain—We have previously shown that, in the absence of GIIβ, GIIα folds into an active subunit that can hydrolyze the small substrate analog pNPG but is unable to efficiently hydrolyze glucose from *N*-glycans *in vivo* or *in vitro* (14). We developed a complementation assay and showed that a mixture of microsomes derived from mutant *S. pombe* cells devoid of GIIα or GIIβ subunits could partially restore the level of GII deglucosylation of $Glc_1Man_9GlcNAc$ observed in microsomes from wild-type cells (14). Using this assay, addition of recombinant GIIβ dramatically increased the Glc trimming from $Glc_1Man_9GlcNAc$ of *S. pombe* microsomes lacking GIIβ (Fig. 3*A*). To determine whether the isolated MRH domain of *S. pombe* GIIβ (amino acids 357–450; Fig. 2) was functional when expressed in *E. coli*, we used the same assay. Addition of up to 50 times more molar amounts of the recombinant GIIβ MRH domain (compared with full-length GIIβ) to microsomes containing only GIIα subunits did not enhance GII enzymatic activity (Fig. 3*A*). This result was expected as the MRH domain lacks the portion of the GIIβ subunit responsible for the interaction between GIIα and GIIβ subunits (GIIβ G2B domain; Fig. 2*A*) (15, 16). However, addition of GIIβ MRH domain inhibited GII activity in mixtures of microsomes containing GIIα plus GIIβ subunits in a dose-dependent manner (Fig. 3*B*), thus strongly suggesting that the recombinant GIIβ MRH domain was sequestering the high mannose glycan portion of the substrate. In contrast, BSA had no effect (Fig. 3*B*).

To directly assess the ability of GIIβ MRH domain to bind high mannose-type glycans, SPR experiments were conducted in which a glycoprotein, GAA, was immobilized and GIIβ MRH domain was flowed over the surface of the sensor chip. The immobilized recombinant GAA contains exclusively high mannose-type glycans with 8.35 mannose residues on average per glycan (36). In these studies, we used a robust *E. coli* expression system in which recombinant GIIβ MRH domain was purified from insoluble inclusion bodies and refolded. The results dem-

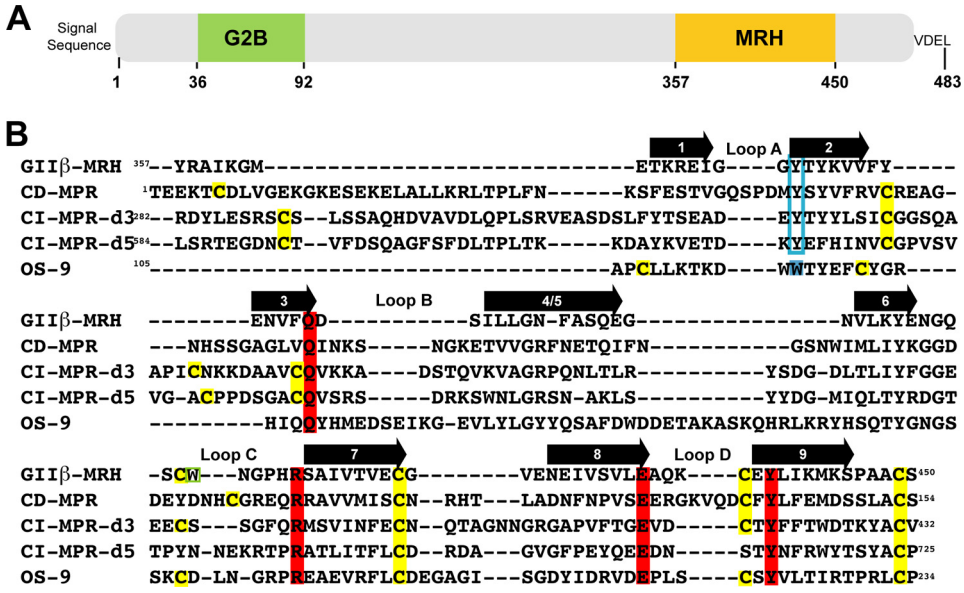

FIGURE 2. **Comparison of glycan-binding MRH domains from GIIβ, CD-MPR, CI-MPR, and OS-9**. *A*, schematic representation of the domain organization of *S. pombe* GIIβ. The mature polypeptide lacking the predicted 23-residue signal sequence is shown. *B*, structure-based sequence alignment of MRH domains from *S. pombe* GIIβ, bovine CD-MPR, domains 3 and 5 of the bovine CI-MPR, and human OS-9. The secondary structural elements of GIIβ with *arrows* representing β-strands and loops A–D are indicated. In contrast to GIIβ and OS-9, the MPRs contain additional elements at their N terminus: domains 3 and 5 of the CI-MPR contain two β-strands, whereas the CD-MPR contains a single α-helix (see Fig. 5*D*). Cysteine residues are shaded in *yellow*. Residues that are within hydrogen-bonding distance of the mannose ring as determined by the crystal structure of OS-9 (Protein Data Bank code 3AIH), domains 1–3 (Protein Data Bank code 1SZ0) of the CI-MPR, and the CD-MPR (Protein Data Bank code 1C39) and the NMR solution structure of domain 5 (Protein Data Bank code 2KVA) of the CI-MPR and have been shown to be essential for Man-6-P binding by mutagenesis studies (*i.e.* Gln, Arg, Glu, and Tyr) are shaded in *red*. Trp-118 of OS-9 that along with Trp-117 is hypothesized to be involved in Manα1,6Man linkage recognition (7) is shaded in *cyan*. The corresponding tyrosine residue in GIIβ, domains 3 (*d3*) and 5 (*d5*) of the CI-MPR, and the CD-MPR are *boxed* in *cyan*. Trp-409 of GIIβ is *boxed* in *green*.

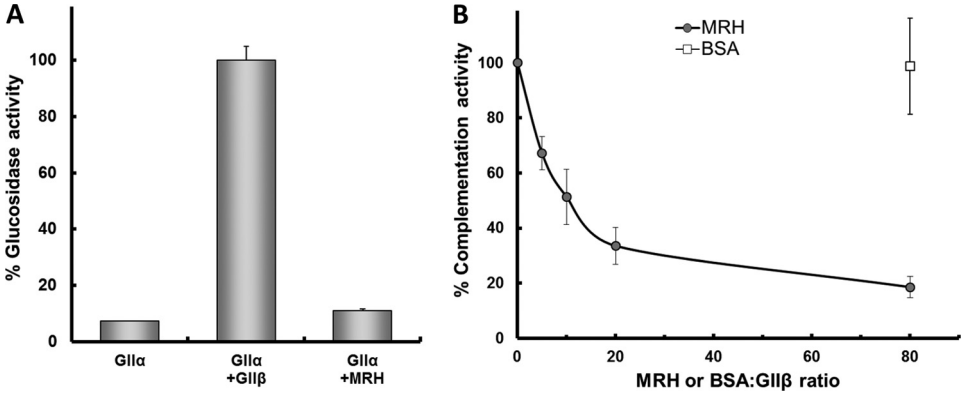

FIGURE 3. **The MRH domain of GIIβ represents a fully functional glycan binding unit.** The MRH construct was expressed as a SUMO fusion protein in *E. coli* and purified and refolded from inclusion bodies prior to proteolytic removal of the SUMO peptide. Mature GIIβ was expressed in an *E. coli* strain that allows disulfide bridge formation (BL21 C3030) as a soluble His_6-tagged fusion protein (*A* and *B*). *A*, MRH alone is unable to replace GIIβ-mediated restoration of glucosidase activity. A source of GIIα (125 μg of microsomes from Δ*GIIαβ S. pombe* cells transformed with pGIIαVDEL) was incubated alone (*GIIα*), with 125 ng of recombinant GIIβ (*GIIα* + *GIIβ*), or with 1.25 μg of recombinant MRH (*GIIα* + *MRH*). GII activity was measured as the amount of glucose released after a 15-min incubation with [^{14}C-Glc]$Glc_1Man_9GlcNAc$ (14). The amount of glucose released in the GIIα + GIIβ condition was set at 100%. *B*, MRH competes with GIIβ for binding to high mannose *N*-glycans. Microsomes from Δ*GIIαβ S. pombe* cells transformed with pGIIαVDEL were incubated as in *A* with 150 ng of recombinant GIIβ (*GIIα* + *GIIβ*) or along with the indicated amounts of MRH/GIIβ or BSA/GIIβ ratios. The amount of glucose released in the GIIα + GIIβ condition was set at 100%. *Error bars* represent S.D.

onstrate that the MRH domain binds high mannose-type glycans with an estimated K_d of 120 μM (Fig. 4*A*). The affinity measured by SPR, although lower, is comparable with the affinities (K_d = ~20–80 μM) determined for a tetrameric form of the human GIIβ MRH domain using frontal affinity chromatography and 2-aminopyridine-labeled glycans (13). Differences may be due to differences between species, between substrates, in the analytical methods used for measurements, and between monomeric and tetrameric avidities of the protein preparations. Taken together, these results demonstrate that the refolded recombinant *S. pombe* GIIβ MRH domain is functional in binding high mannose *N*-glycans and thus is suitable for structural analyses (13).

GIIβ Lectin Domain Adopts the Conserved MRH Fold—The 300-kDa cation-independent MPR (CI-MPR) contains 15 extracellular MRH domains, three of which bind phosphomannosyl residues (domains 3, 5, and 9), whereas the smaller cation-dependent MPR (CD-MPR) contains a single MRH domain. Our crystal/solution structures of the CD-MPR and domains 1–3 and domain 5 of the CI-MPR have been determined in the

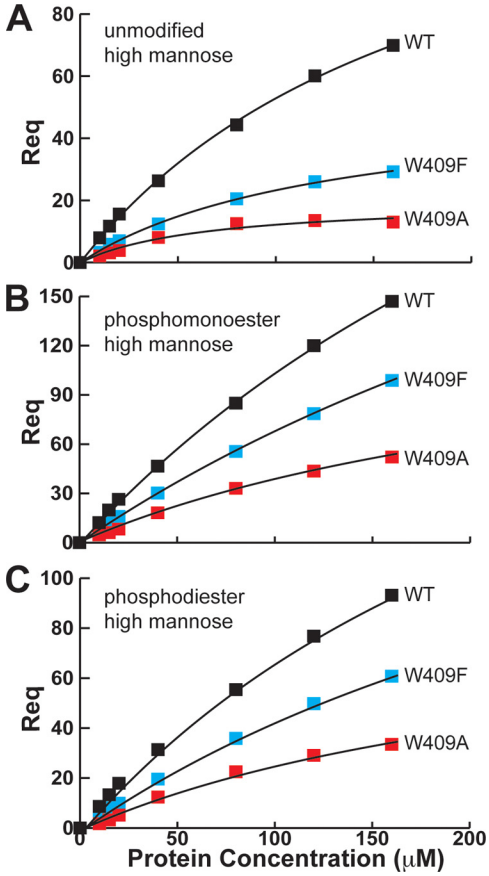

FIGURE 4. **SPR analyses of GIIβ MRH domain binding to a glycoprotein, GAA.** Purified GIIβ MRH domain was flowed over the surface of a CM5 sensor chip immobilized with GAA containing high mannose *N*-glycans (*A*), high mannose *N*-glycans with phosphomonoesters (*B*), or high mannose *N*-glycans with phosphodiesters (*C*). The response at equilibrium (R_{eq}) to the GAA surfaces is plotted *versus* the concentration of protein (0, 5, 10, 20, 40, 80, 120, and 160 μM) and fitted as described previously (35). GAA contains exclusively high mannose-type glycans with 8.35 mannose residues on average per glycan and either 0.25 mol of Man-6-P/mol of glycan (phosphomonoester) or GlcNAc-modified glycan (phosphodiester) (36). The mean and S.D. from three independent analyses are as follows for the high mannose, phosphomonoester, and phosphodiester surfaces, respectively: wild type, 121 ± 35, 115 ± 16, and 111 ± 28 μM; W409A, 294 ± 219, 203 ± 44, and 395 ± 44 μM; W409F, 193 ± 72, 176 ± 35, and 212 ± 73 μM.

TABLE 1
Refinement statistics for the GIIβ MRH domain NMR ensemble of 20 structures
r.m.s., root mean square.

Experimental constraints	
Distance constraints	
Long	737
Medium ($1 < (i - j) \leq 5$)	260
Sequential ($(i - j) = 1$)	465
Intraresidue ($i = j$)	338
Total	1,800
Dihedral angle constraints (ϕ and ψ)	130
Average atomic r.m.s.d. to the mean structure (Å)	
Residues	358–450
Backbone (Cα, C′, N)	0.39 ± 0.06
Heavy atoms	0.83 ± 0.09
Deviations from idealized covalent geometry	
Bond length r.m.s.d. (Å)	0.019
Torsion angle violation r.m.s.d. (°)	1.4
Constraint violations	
NOE distance	
Number >0.5 Å	0.0 ± 0
r.m.s.d. (Å)	0.020 ± 0.001
Torsion angle violations	
Number >5°	0.0 ± 0
r.m.s.d. (°)	0.734 ± 0.089
WHATCHECK quality indicators	
Z-score	0.34 ± 0.15
r.m.s. Z-score	
Bond lengths	0.85 ± 0.02
Bond angles	0.67 ± 0.02
Bumps	0.0 ± 0
Lennard-Jones energy[a] (kJ mol^{-1})	−2,261 ± 47
Ramachandran statistics (% of all residues)	
Most favored	83.5 ± 1.8
Additionally allowed	13.7 ± 1.7
Generously allowed	1.3 ± 0.9
Disallowed	1.5 ± 0.5

[a] Nonbonded energy was calculated in Xplor-NIH.

presence of a carbohydrate ligand (35, 37). These structures allowed us to identify four conserved residues (Gln, Arg, Glu, and Tyr), which interact with the 2-, 3-, and 4-hydroxyl groups of the mannose ring, that are essential for Man-6-P recognition by the MRH domains of MPRs. These four residues, which form the binding pocket, are also conserved in the GIIβ MRH domain (Fig. 2*B*). Mutagenesis of the analogous residues in *S. pombe* GIIβ MRH domain abolished the ability of GIIβ to enhance glycan trimming by GII in live cells (14). Previous studies showed that the GIIβ MRH domain recognizes mannose residues in the B and/or C arms of *N*-glycans as the absence of these mannose residues in the glycan prevents trimming of the glucose in arm A by GII both *in vitro* and in living cells (11–13, 15, 38). The differences in substrate specificity between this ER glycoprotein folding quality control enzyme and OS-9, a receptor involved in ER-associated degradation, prompted us to obtain the solution structure of the isolated GIIβ MRH domain from *S. pombe* using three-dimensional NMR techniques. Sample conditions were optimized as described under "Experimental Procedures" to obtain high quality spectra of $^{15}N/^{13}C$-labeled recombinant GIIβ MRH domain at pH 7.2 (Table 1).

S. pombe GIIβ is the shortest (89 residues; Fig. 2) of the MRH domain structures that have been determined to date (eight of the 15 MRH domains of CI-MPR (35, 39–41), CD-MPR (42), and OS-9 (7)). GIIβ MRH domain folds into a flattened nine-stranded β-barrel comprising two antiparallel β-sheets oriented orthogonally over one another (Fig. 5, *A–C*). This structure is similar to the structures reported for the MRH domains of the MPRs and OS-9 with the overall fold of GIIβ MRH domain being most similar to that of OS-9 (r.m.s.d. = 1.32 Å; 85 Cα atoms) (Fig. 5*D*). Both OS-9 and GIIβ adopt a compact β-barrel structure due to their lack of ~20 amino acids present at the N terminus of the CD-MPR and CI-MPR MRH domains that form either an α-helix or two to three short β-strands, respectively. However, *S. pombe* GIIβ MRH domain loops A and B as well as β-strands 4/5 and 6 are significantly shorter than those in OS-9 (Fig. 5*D*). Additionally, *S. pombe* GIIβ MRH domain contains only four cysteine residues in contrast to the six (CD-MPR, CI-MPR domain 5, and OS-9) or eight (domains 3 and 9 of the CI-MPR) cysteine residues found in the other glycan-binding MRH domains. The absence of the N-terminal disulfide bond in *S. pombe* GIIβ MRH domain that is found in other MRH domains as well as other species of GIIβ does not appear to affect the overall fold of the domain. The structural stability provided by the N-terminal disulfide bond may be

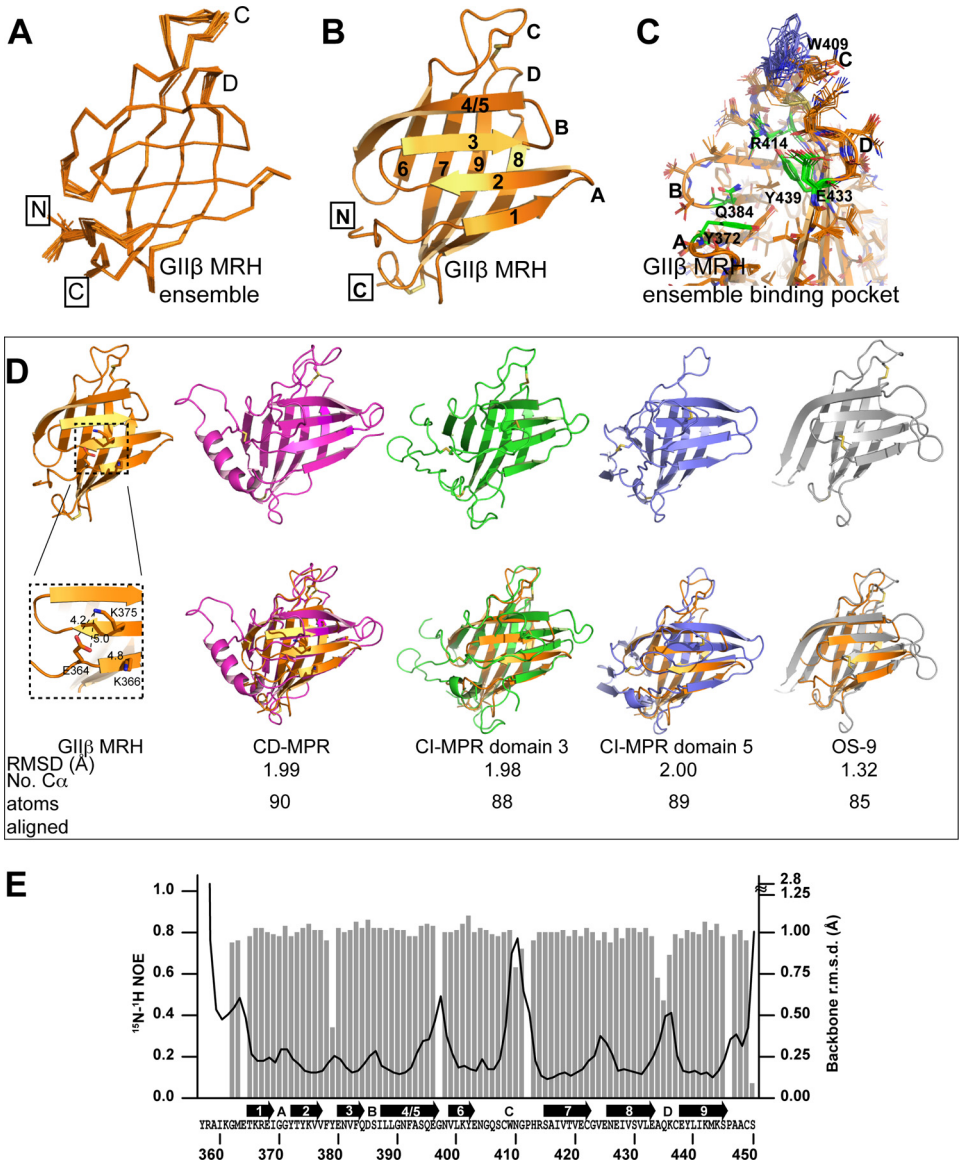

FIGURE 5. **Solution structure of GIIβ MRH domain and comparison with solved structures of other MRH domain-containing proteins.** *A*, superimposition of the backbone atoms of the 20 lowest energy structures of GIIβ MRH domain ensemble. N and C termini are *boxed*, and loops C and D are labeled. *B*, ribbon diagram of the representative conformer (derived from an ensemble of 20 conformers) of GIIβ MRH domain in a ligand-free state is shown (Protein Data Bank code 2LVX). β-Strands are *numbered* from the N to the C terminus, and loops A through D are labeled. Disulfide bonds are shown in *yellow*. *C*, close-up view of the GIIβ MRH domain binding pocket. The backbone atoms of the lowest energy conformer are represented by the *orange ribbon*, and the side chains of the ensemble members are shown as *lines*. The essential residues within the proposed binding pocket are shown in *green*, whereas Trp-409, which shows high mobility, is shown in *blue*. Loops A, B, C, and D are labeled. *D*, comparison of GIIβ MRH domain with solved structures of MRH domain-containing proteins. *Upper panel*, ribbon diagram of the representative conformer (derived from an ensemble of 20 conformers) of GIIβ MRH domain in a ligand-free state (*orange*; Protein Data Bank code 2LVX) and of the MRH domains of CD-MPR (*pink*; Protein Data Bank code 1C39), domain 3 of CI-MPR (*green*; Protein Data Bank code 1SZ0; Man-6-P), domain 5 of CI-MPR (*blue*; Protein Data Bank code 2KVB), and OS-9 (*gray*; Protein Data Bank code 3AIH). Disulfide bonds are shown in *yellow*. Below the ribbon diagram of GIIβ MRH domain is a close-up view of the N-terminal region in which electrostatic interactions replace a disulfide bond found in the other MRH domains. The distance in angstroms among the side chains of Glu-364, Lys-366, and Lys-375 is shown. Figures were generated using PyMOL (54). *Lower panel*, superimposition of the structure of the GIIβ MRH domain with each of the structures shown in the *upper panel*. CD-MPR aligns over 90 Cα atoms with an overall r.m.s.d. of 1.99 Å. CI-MPR domain 3 aligns over 88 Cα atoms with an overall r.m.s.d. of 1.98 Å. CI-MPR domain 5 aligns over 89 Cα atoms with an overall r.m.s.d. of 2.00 Å. OS-9 aligns over 85 Cα atoms with an overall r.m.s.d. of 1.32 Å. *E*, backbone (Cα) r.m.s.d. values of the ensemble for GIIβ MRH domain (*solid line*) and ^{15}N-^{1}H heteronuclear NOE values (*bars*) are plotted as a function of amino acid sequence. Secondary structural elements are also shown. The N-terminal five residues and Gly-397 were unassigned.

replaced in *S. pombe* GIIβ MRH domain with electrostatic interactions between Glu-364 and Lys-366 and Lys-375 located on strands 1 and 2, respectively (Fig. 5*D*).

The dynamic nature of the GIIβ MRH domain was evaluated by a comparison of r.m.s.d. values calculated between corresponding Cα atoms for each member of the structure ensemble and ^{15}N-^{1}H heteronuclear NOE experiments. Unlike domain 5 of the CI-MPR, which showed overall greater mobility as assessed by ^{15}N-^{1}H heteronuclear NOE values (35), the compact nature of GIIβ MRH domain with shortened loops between strands 1 and 2 and strands 4/5 and 6 coupled with the presence of a disulfide tethering loops C and D together results in comparably lower flexibility in the molecule in the absence of ligand and r.m.s.d. values more similar to domain 5 of CI-MPR

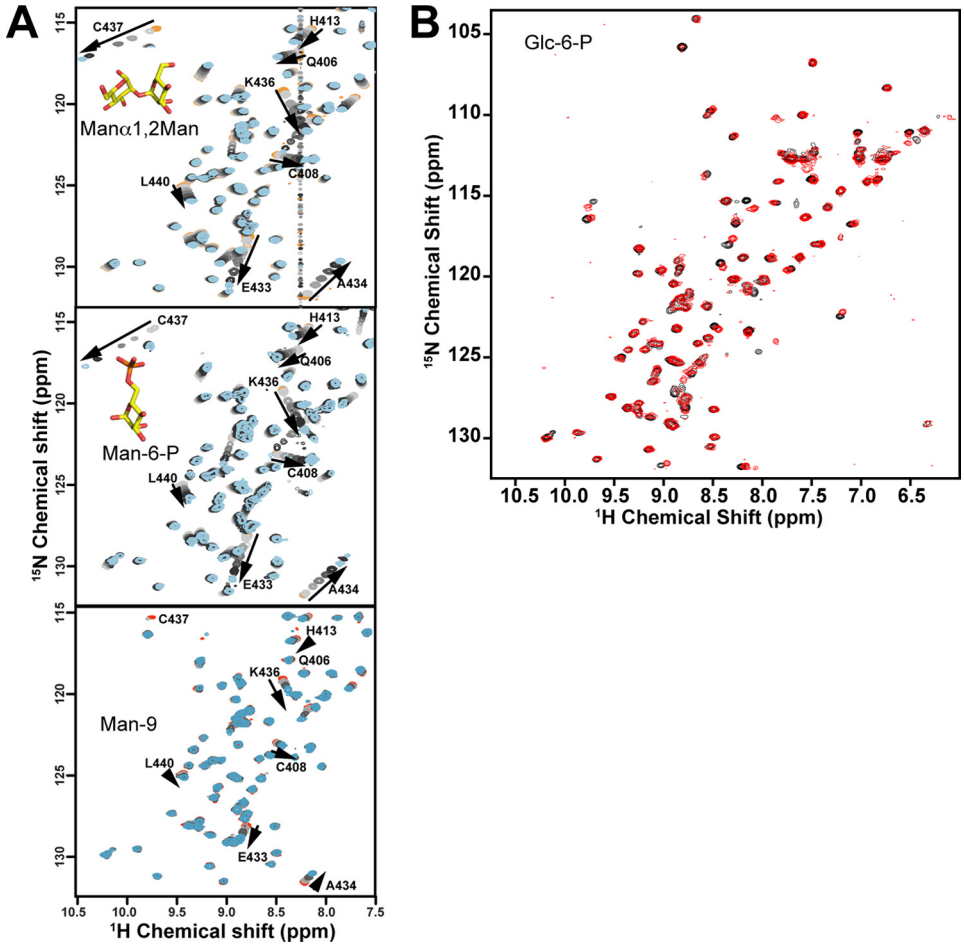

FIGURE 6. **HSQC spectra of GIIβ MRH domain with Manα1,2Man, Man-6-P, $Man_9GlcNAc$, or Glc-6-P.** Selected regions of ^{15}N-^{1}H HSQC spectra GIIβ MRH domain collected with increasing amounts of disaccharide Manα1,2Man (*top*), the monosaccharide Man-6-P (*middle*), and the glycan $Man_9GlcNAc$ (*bottom*) (*A*) or Glc-6-P (*B*) are shown. The spectrum of 0.1 mM GIIβ MRH domain was collected in the presence of ligands in concentrations ranging from 0 to 400 mM added in seven aliquots of Manα1,2Man and Man-6-P, in three aliquots (0.4, 0.8, and 1.6 mM) of $Man_9GlcNAc$, or a single aliquot of 200 mM for Glc-6-P (color code: *orange*, 0 mM; *cyan*, highest concentration reached with each ligand; from *gray* to *black*, intermediate concentrations).

in the ligand-bound state. These results demonstrate that the structure of GIIβ MRH domain is relatively constrained with the exception of residues in loops C and D (Fig. 5, *A*, *C*, and *E*).

Binding Pocket and Specificity of GIIβ MRH Domain—To map the binding pocket of GIIβ MRH domain with carbohydrates, increasing amounts of the disaccharide Manα1,2Man, the monosaccharide Man-6-P or glucose 6-phosphate (Glc-6-P), or the glycan $Man_9GlcNAc$ were added to $^{13}C/^{15}N$-labeled sample, and changes in chemical shifts of amide groups located in either backbone or side chains were monitored. These ligand titrations were also used to (i) determine whether pure glycan and simple carbohydrate molecules bound specifically to the conserved MRH domain recognition site and (ii) test the hypothesis that the GIIβ MRH domain selectively recognizes mannose in contrast to glucose. An overlay of spectra acquired in the presence of increasing concentrations of Manα1,2Man, Man-6-P, or $Man_9GlcNAc$ demonstrated progressive chemical shift changes for residues either within or adjacent to the proposed binding pocket (Fig. 6*A*). The weighted changes in combined $^{1}H/^{15}N$ chemical shift perturbations were used to determine relative binding affinities for Manα1,2Man (K_d = 65 ± 3 mM), Man-6-P (K_d = 77 ± 7 mM), and $Man_9GlcNAc$ (K_d = 2.6 ± 0.4 mM) (Figs. 7, *A*–*C*). These results show a significantly higher relative affinity (~25-fold) for the larger glycan than for the disaccharide. The ability to recognize both mannose and Man-6-P suggests that substitution at the 6-position (*i.e.* hydroxyl or phosphate) does not constitute a major recognition determinant for GIIβ MRH domain. This hypothesis is further validated by SPR analyses show that K_d values for GIIβ MRH domain interacting with an immobilized glycoprotein bearing high mannose (Fig. 4*A*), phosphomonoesters (Fig. 4*B*), or phosphodiesters with a GlcNAc on the 6′-OH group of the mannose (Fig. 4*C*) are similar. Thus, the GIIβ MRH domain differs from the P-type lectin MRH domains of the MPRs that exhibit a preference to bind either phosphate on the 6-hydroxyl of mannose (domain 3 of the CI-MPR and CD-MPR) or a phosphodiester (domain 5 of the CI-MPR) (36) and from human OS-9, which binds mannose but not Man-6-P (43).

To probe whether the GIIβ MRH domain can recognize glucose, ^{15}N-^{1}H HSQC collected in the presence of Glc-6-P, which differs from Man-6-P only in the positioning of the 2′-OH group, produced chemical shift perturbations localized to the same regions as Man-6-P although to a significantly lower extent (Figs. 6*B* and 7*D*). These weak interactions observed with Glc-6-P demonstrate that the axial 2′-OH present in mannose is a key recognition determinant for the GIIβ MRH

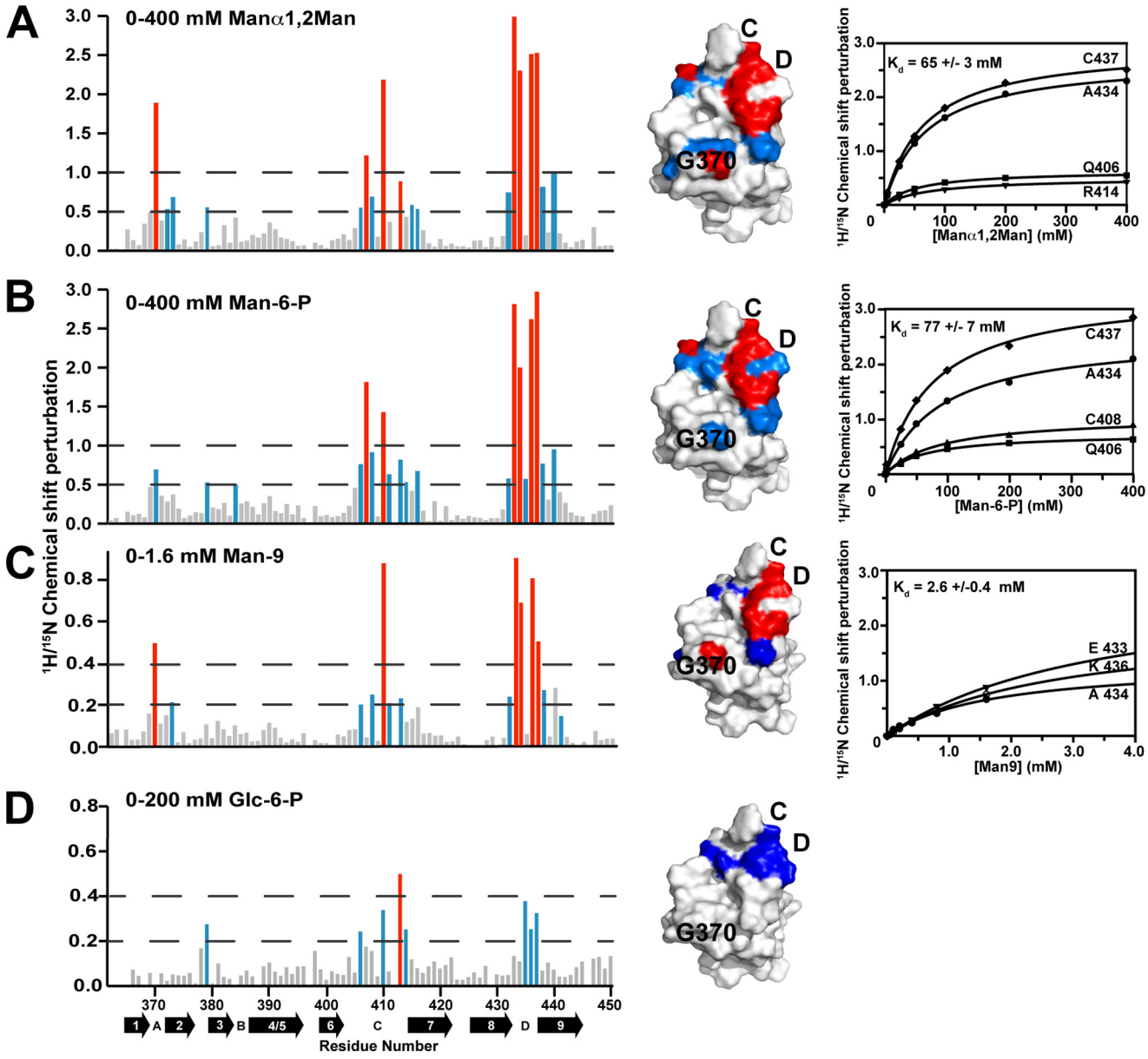

FIGURE 7. **Interaction of GIIβ MRH domain with Manα1,2Man, Man-6-P, $Man_9GlcNAc$, or Glc-6-P.** The spectrum of 0.1 mM GIIβ MRH domain was collected in the presence of ligands and is shown in Fig. 6. ^{15}N-^{1}H chemical shift perturbations for Manα1,2Man (*A*), Man-6-P (*B*), $Man_9GlcNAc$ (*C*), or Glc-6-P (*D*) were plotted against the residue number of GIIβ MRH domain (*left panels*). Secondary structural elements are listed below the sequence numbers. Missing values correspond to proline residues or residues not observed in the ^{15}N-^{1}H HSQC spectra. *Middle panels* depict chemical shift mapping on the GIIβ MRH domain structure. The molecular surface highlighted in *red* corresponds to amino acids with the largest chemical shift perturbations (>1), whereas those colored in *cyan* represent moderate perturbations (0.5). *Right panels*, chemical shift differences for the eight selected residues (labeled in *A*) were calculated as $\Delta\delta = [(5 \times \Delta NH\delta)^2 + \Delta N\delta]^{1/2}$. Representative curves for four of the eight residues monitored for the Manα1,2Man and Man-6-P titrations and curves for the three residues monitored for the $Man_9GlcNAc$ titration are shown. Dissociation constants (K_d) were determined from monitoring changes in the chemical shift of the eight selected residues as described under "Experimental Procedures."

domain. Although K_d values of 65–77 mM for the monosaccharide Man-6-P and disaccharide Manα1,2Man may not equate to the binding interactions occurring between GII and its heterogeneous population of *N*-glycan-containing substrates in the ER, the results demonstrate that GIIβ MRH domain interacts preferentially with mannose. Taken together, the observation that the affinity for the monosaccharide Man-6-P and the disaccharide Manα1,2Man are similar along with the ability of Glc-6-P to cause specific but very low chemical shift perturbations supports the structural findings that GIIβ MRH domain has a shallow binding pocket (see below) that accommodates preferentially a single mannose residue. From a functional standpoint, the inability of GIIβ MRH domain to efficiently recognize glucose eliminates the potential for the β-subunit to compete with the catalytic α-subunit of GII for glucose present in arm A of the *N*-glycan.

Mannose Binding Pocket—GIIβ MRH domain contains the four residues (Gln-384, Arg-414, Glu-433, and Tyr-439) known to be essential for Man-6-P binding by the MPRs (Fig. 2*B*), and mutational studies support their involvement in GII activity (13, 14). To evaluate the role these residues play in carbohydrate binding, measurements of weighted differences in com-

bined $^{1}H/^{15}N$ chemical shift perturbations with increasing amounts of ligand were used to map the location of the Manα1,2Man, Man-6-P, and Man$_9$GlcNAc (Fig. 7, *A–C*) binding site to the surface of GIIβ MRH domain. The greatest chemical shift perturbations of the ligands map to an area (loops C and D) corresponding to the known carbohydrate binding sites of CD-MPR, of domains 3 and 5 of the CI-MPR, and of OS-9. Although chemical shift perturbations were observed for residues in the proposed binding pocket, two of the essential ligand binding residues, Gln-384 and Tyr-439, did not show significant changes in chemical shift in the presence of ligand (Fig. 7). We postulate from the structure that the amide protons are unable to shift due to extensive hydrogen bonding with neighboring atoms due to their location in β-strands that are part of the two β-sheets. Residues in loop A experienced slightly greater chemical shift differences in the presence of the larger ligands: a stronger chemical shift perturbation at Gly-370 and additional perturbations for Tyr-372 and Thr-373 were observed (Fig. 7, *A–C*). However, the striking similarity of the chemical shift mapping between the disaccharide and the monosaccharide coupled with their similar affinities supports the lack of an extended binding pocket. This notion is further supported by the observation that the branched Man$_9$GlcNAc glycan, which exhibited ~25-fold higher affinity than Man-6-P or Manα1,2Man, failed to produce additional measurable chemical shift perturbations at the highest concentration used (Fig. 7). Although these structural analyses failed to identify additional protein contacts to explain the increased affinity observed for the Man$_9$GlcNAc glycan compared with the smaller ligands, the longer glycan may have constrained the terminal and penultimate mannose into an optimal conformation for binding. Furthermore, the observed ~20-fold higher affinity of GIIβ MRH domain for a glycoprotein bearing high mannose-type *N*-glycans compared with a glycan free in solution (K_d = ~120 μM (Fig. 4*A*) *versus* K_d = 2.6 ± 0.4 mM (Fig. 7*C*); SPR data were obtained with glycoproteins, whereas NMR data were obtained using free glycans) may be the result of protein-induced restrictions that increase the percentage of *N*-linked glycans in the optimal conformation for binding and/or of differences in the principles of the methods used to estimate affinities.

The lumen of the ER is a crowded environment with protein concentrations up to 200–300 mg/ml (44). Given the high substrate concentration for the ER quality control machinery in which transient interactions occur, it is reasonable to expect that the affinities of ER MRH domains for glycoproteins in this environment would not be as high as those of the Golgi MRH domains in which the Man-6-P receptors must capture the very low abundance of lysosomal enzymes for transportation to late endosomes. The limited interactions with mannose and the failure of either Man$_9$GlcNAc or a disaccharide to produce submillimolar binding affinities are likely a direct consequence of the shallowness of this binding pocket relative to the other MRH binding pockets solved to date (CD-MPR, domains 3 and 5 of CI-MPR, and OS-9) (Fig. 8). In *S. pombe*, this shallow mannose binding region is due to the dramatically shortened loop B relative to other species and the positioning of loop C more distally from the essential residues in the pocket, thereby allowing the binding site to accommodate mannose modified at the 6-hydroxyl (*i.e.* phosphate and GlcNAc) (Figs. 5 and 8). Notably, the four residues considered essential for mannose binding (Gln-384, Arg-414, Glu-433, and Tyr-439) overlay well with those in the other four MRH domains (Fig. 8). Because the ligand-bound crystal structures of domain 3 of the CI-MPR, OS-9, and the CD-MPR demonstrate directly that the common positioning of these four essential residues results in a nearly identical positioning of the mannose ring within the binding pocket, we predict that the mode of mannose binding by the GIIβ MRH domain to these four residues will be essentially the same.

Although the four mannose-interacting residues are conserved among these MRH domains, other structural features must exist to explain the different preferences displayed by these proteins for high mannose-type glycans (45). For example, OS-9 contains a double tryptophan motif that is proposed to determine the α1,6-linkage specificity of OS-9 (7). These residues form an extended surface to accommodate the penultimate and prepenultimate mannose residues of one arm of the glycan (see Fig. 8) (7). In contrast, GIIβ MRH domain contains a conserved tyrosine residue (Tyr-372; strand β2) as observed in the MPRs (Figs. 2*B*, *cyan*, and 8). This tyrosine has been proposed by Satoh *et al.* (7) to be the residue responsible for conveying α1,2-linkage specificity by the MPRs. However, we have crystallized domain 3 of the CI-MPR with a Manα1,3Man in the binding pocket (39), suggesting that this tyrosine (Tyr-324) in domain 3 is not involved in specifying a linkage preference for α1,2-containing ligands. Furthermore, the side chain of Tyr-372 of the GIIβ MRH domain, unlike that of the MPRs, is oriented 90° away from the binding pocket such that the hydroxyl group is unable to interact with the glycosidic linkage of the ligand (Fig. 8). The significant number of NOE constraints for this residue along with the rest of the molecule (average of 21 NOE constraints per residue) further validates the positioning of the side chain of Tyr-372 in the GIIβ MRH domain structure determined in the absence of ligand. However, we cannot exclude the possibility that in the presence of ligand the side chain of Tyr-372 may reposition. Thus, additional studies are needed to evaluate the role of this conserved residue in the MPRs and GIIβ.

Role of a Conserved Trp-409 among GIIβ MRH Domains—A comparative analysis of the residues within and surrounding the proposed binding pocket revealed another residue that is highly conserved and unique to the GIIβ MRH domain. Trp-409, which is located in loop C, is absolutely conserved among 77 of the 79 homologs analyzed (Fig. 8) and is not present in the other MRH domains (Fig. 2*B*). Our initial assessment of the role of the conserved Trp-409 was performed in the context of the isolated MRH domain. Mutants containing conservative (W409F) or non-conservative (W409A) substitution of Trp-409 were generated, and ^{15}N-labeled proteins were evaluated. ^{15}N-^{1}H HSQC experiments show that both constructs are folded, which is reflected in their similar ^{15}N-^{1}H HSQC spectra as the wild-type protein (Fig. 9*A*). Furthermore, addition of 50 mM Manα1,2Man disaccharide to the W409A ^{15}N-labeled sample resulted in chemical shift perturbations on the order of those found for similar concentrations of the wild-type protein

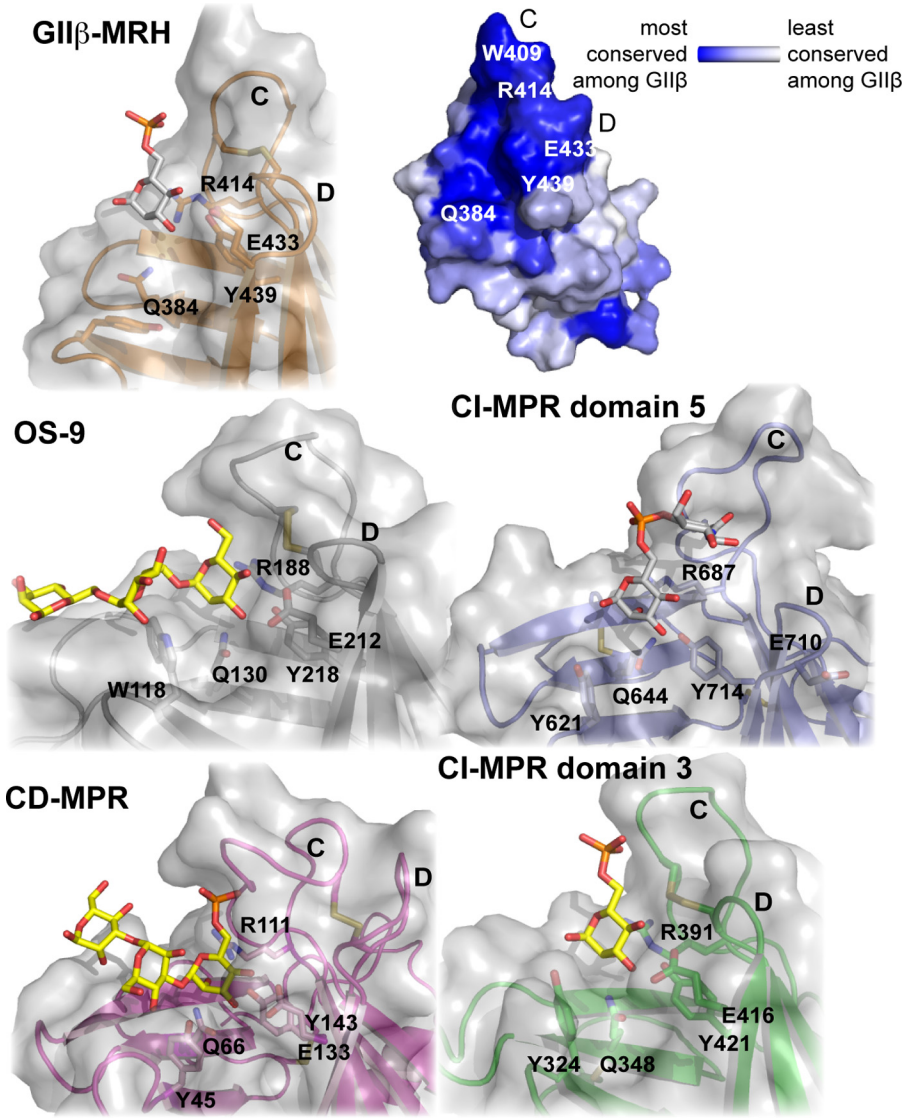

FIGURE 8. **Close-up view of MRH binding pockets**. The carbohydrate binding sites of GIIβ MRH domain (*orange*; Protein Data Bank code 2LVX), domain 3 of CI-MPR (*green*; Protein Data Bank code 1SZ0), domain 5 of CI-MPR (*blue*; Protein Data Bank code 2KVB), OS-9 (*gray*; Protein Data Bank code 3AIH), and CD-MPR (*pink*; Protein Data Bank code 1C39) show the four essential mannose-binding residues along with the proposed linkage-sensing Tyr or Trp. Modeled ligands based on superimposition of the essential residues to a structure of known binding site (Man-6-P for GIIβ MRH domain and methyl-Man-P-GlcNAc for CI-MPR domain 5) are depicted in *gray*. Structures solved in the presence of bound ligands (Man-6-P for CI-MPR domain 3, Manα1,6Manα1,6Man for OS-9, and pentamannosyl phosphate for CD-MPR) are shown in *yellow*. Loops C and D are labeled in all structures, and disulfide bridges are shown in *yellow*. Molecular surfaces are shown over the ribbon schematic. A molecular surface of GIIβ MRH domain colored by species conservation as determined by ConSurf is also shown. Seventy-nine homologs were used in the calculation. Inspection of the GIIβ MRH domain ^{15}N-^{1}H HSQC spectra in the presence of increasing concentrations of Man-6-P *versus* Manα1,2Man revealed chemical shift perturbations consistent with location of the modeled ligand Man-6-P as amide chemical shift changes in Gln-435 residing in loop D as well as Gly-411 in loop C were observed.

(Fig. 9*B*). In addition, SPR experiments show that W409A and W409F bound immobilized glycoproteins bearing high mannose (Fig. 4*A*), phosphomonoesters (Fig. 4*B*), or phosphodiesters bearing a GlcNAc on the 6′-OH group of the mannose (Fig. 4*C*) with a slight decrease in affinity (within 3.5-fold) compared with the wild-type protein. Thus, substitution of Trp-409 does not dramatically lower binding affinity toward glycans in the context of the isolated MRH domain.

To study the influence of Trp-409 of GIIβ MRH domain in GII activity, we mutated Trp-409 in the full-length GIIβ (W409A or W409F), expressed the wild-type or mutated GIIβ in *S. pombe* cells lacking endogenous GIIβ (Δ*GIIβ*), and measured GII activity toward both the small substrate analog pNPG and [^{14}C-Glc]$Glc_1Man_9GlcNAc$ in microsomal fractions obtained from the mutant cells. Results presented in Fig. 10*A* show that although the influence of Trp-409 in GIIβ-mediated GIIα activity enhancement was not as strong as mutation of the conserved residues (Gln, Arg, Glu, and Tyr) that interact with the 2-, 3-, and 4-hydroxyl groups of the mannose ring (Fig. 2*B*), mutation of Trp-409 precluded full GII activity toward *N*-glycans *in vitro*. We have reported previously that microsomal GII activity using pNPG reflects ER GIIα content (14). Reduced GII activity observed in cells expressing Trp-409-mutated GIIβ is not due to a reduced ER GIIα content as the activity toward pNPG was not reduced in mutant GIIβ W409A or GIIβ W409F (Fig. 10*A*). Moreover, Western blot analyses show normal GIIα

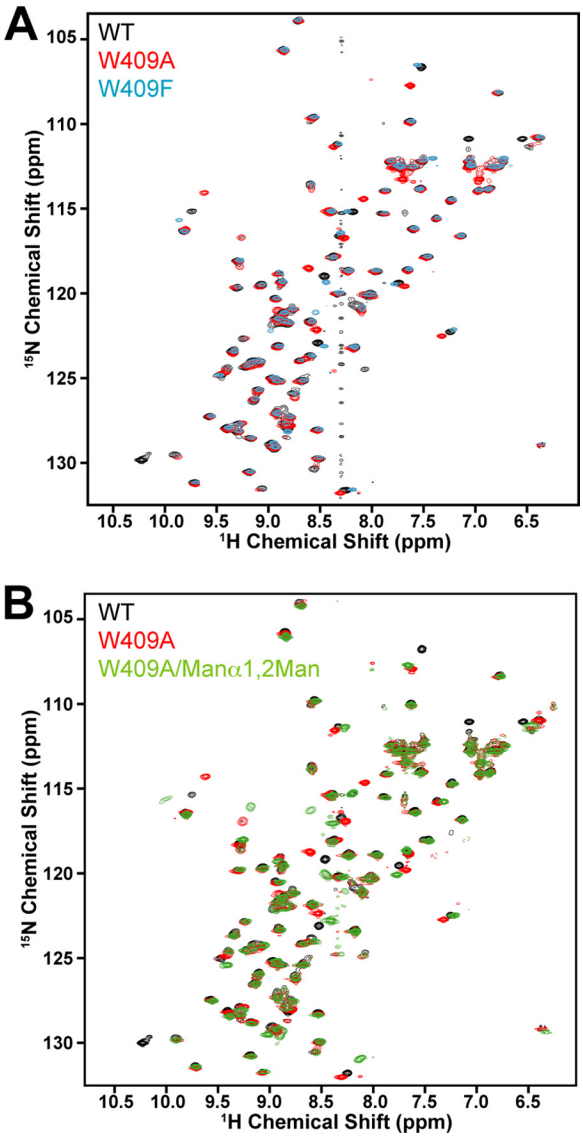

FIGURE 9. **Comparison of two-dimensional HSQC spectra of wild-type and mutant recombinant GIIβ MRH domain.** *A*, overlay of ^{15}N-^{1}H HSQC spectra from wild-type (*black*) or mutant (W409A, *red*; W409F, *cyan*) GIIβ MRH domain. *B*, overlay of ^{15}N-^{1}H HSQC spectra from wild-type (*black*) or mutant (W409A, *red*) GIIβ MRH domain in the absence of ligand. The ^{15}N-^{1}H HSQC spectrum of W409A collected in the presence of 50 mM Manα1,2Man disaccharide is also shown (*green*).

levels in microsomes (enriched in ER membranes) obtained from GIIβ Trp-409 mutants (Fig. 10*B*).

To determine whether substitution of Trp-409 in the GIIβ MRH domain affects GII glucose trimming activity *in vivo*, we analyzed the *N*-glycan pattern produced by Δ*GIIβ* cells expressing Trp-409 GIIβ mutants (W409A and W409F) and compared it with the *N*-glycan patterns of cells expressing wild-type GIIβ or GIIβ mutated in amino acids predicted to interact with the mannose ring (Y439F and E433Q). Cells were incubated with [^{14}C]Glc for 15 min in the presence of 5 mM DTT, and whole cell *N*-glycans were isolated and analyzed as described under "Experimental Procedures." The total incorporation of the label into the *N*-glycans was linear during the incubation time, and the presence of DTT prevented the passage of glycoproteins to the Golgi, hindering further extension of the recently synthesized *N*-glycans (46). The *N*-glycan patterns obtained from *S. pombe* cells expressing wild-type GIIβ revealed that whereas deglucosylation of the transferred glycan $Glc_3Man_9GlcNac_2$ was so rapid that almost no glucose-containing glycans were detected (Fig. 10*C*) the amount of glucosylated glycans increased in cells expressing GIIβ Trp-409 mutants, although it was not as much of an increase as observed in the GIIβ Y439F mutant (Fig. 10, *D–F*) and as observed previously in Δ*GIIβ* mutants (14). Taken together, the results demonstrate that substitution of Trp-409 in the context of the full-length GIIβ has a moderate to high (60% inhibitory) effect on GII activity.

How Does GIIβ MRH Domain Interact with High Mannose-type Glycans?—Studies both *in vitro* and *in vivo* indicate that residue *k* in arm C plays a more significant role than residue *i* in arm B of the glycan in the enhancement of GII catalytic activity by GIIβ (12–15). To envision how GIIβ enhances the catalytic activity of GII toward glycans, we propose two models that are consistent with the existing biochemical and current structural studies. In the first model, the terminal mannose (residue *k*) of arm C is captured by the shallow binding pocket of the MRH domain of GIIβ defined by the four conserved residues (Gln-384, Arg-414, Glu-433, and Tyr-439). Interaction of the terminal mannose (residue *i*) of arm B with Trp-409 would further constrain the *N*-glycan and facilitate optimal positioning of the glucose-containing arm A near the catalytic site of GIIα (Fig. 11*A*). Visualization of this model was obtained by positioning the terminal mannose residue of arm C of a Man_9 glycan into the MRH binding pocket from the superimposition of the four mannose-binding essential residues (Gln-384, Arg-414, Glu-433, and Tyr-439) with that of domain 3 of CI-MPR containing bound Man-6-P (47). This overlay indicated that the terminal mannose of arm B of the glycan is near loop C and that Trp-409 in loop C could stack against the terminal mannose ring of arm B, thereby providing a bidentate mode of interaction between the MRH domain and two arms of the glycan. Although a previous molecular dynamics simulation of a $Man_9GlcNAc_2$ glycan and NOE analyses indicate that significant flexibility of arms A, B, and C of the glycan (48) complicates such analyses, CH-π-mediated stacking interactions between aromatic residues and carbohydrates are commonly observed in lectins (49, 50), including another ER-resident lectin, malectin, that recognizes the Glcα1,3Glc moiety on Glc_2-*N*-glycans (51). It is intriguing to speculate that Trp-409 is located in a relatively dynamic region of the GIIβ MRH domain (Fig. 5, *A* and *C*) to capture one of the many and related conformers of an *N*-glycan.

In the second model (Fig. 11*B*), Trp-409 interacts with other regions of the β-subunit. Although the GIIβ MRH domain alone is sufficient for binding glycans, its affinity for ligand may be augmented by the presence of the remaining portion of the β-subunit and/or the α-subunit. This enhancement in ligand binding affinity has been reported for both domain 3 (52) and domain 5 (26) of the CI-MPR. Trp-409 of GIIβ could be positioned to interact with residues on adjacent parts of the holoenzyme and act to either stabilize the position of loops C and/or D much like the linker region between domains 1 and 2 does for domain 3 of CI-MPR, resulting in increased affinity for Man-6-P (39, 47), or orient the MRH domain closer to GIIα, resulting

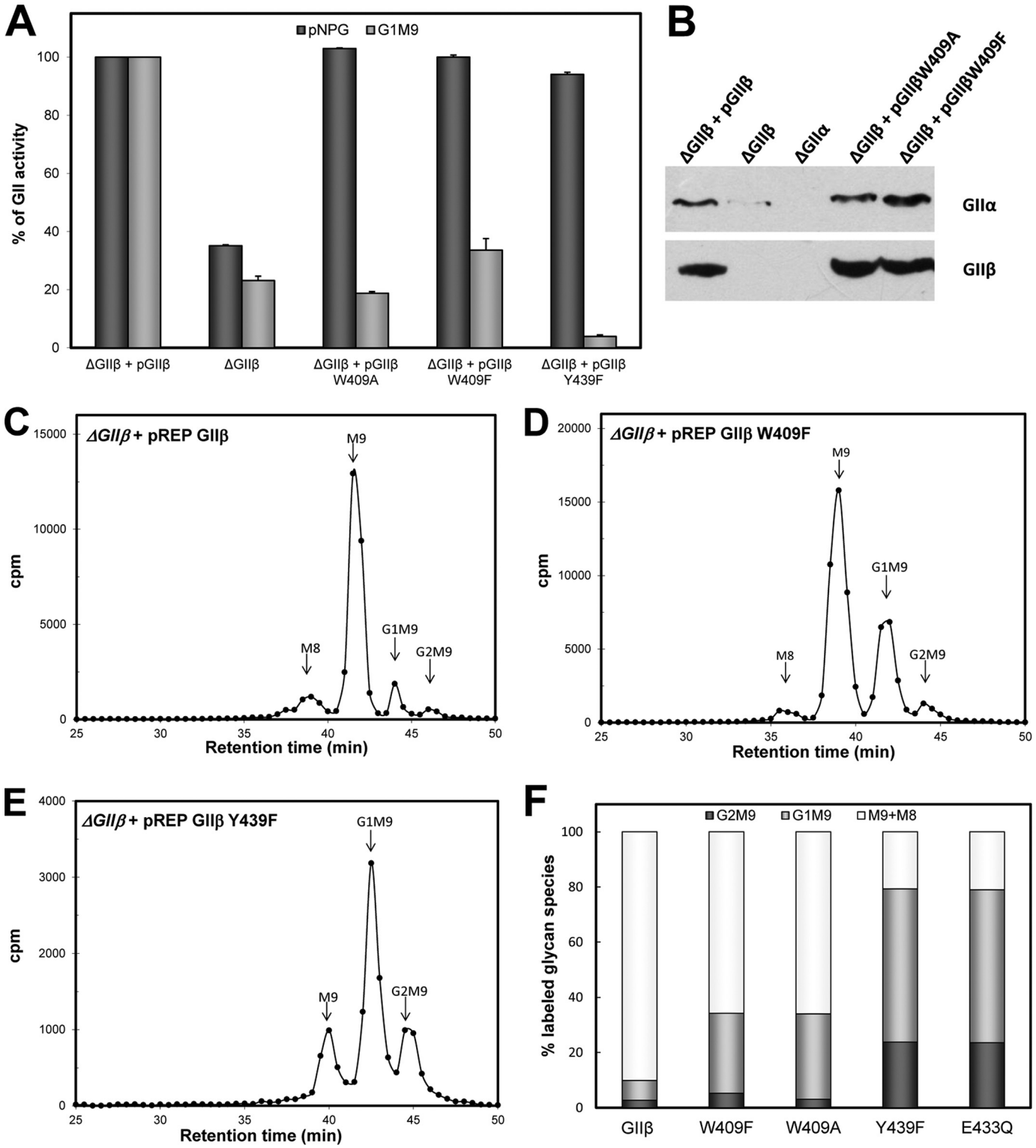

FIGURE 10. **Influence of Trp-409 in GIIβ-mediated GII activity enhancement toward *N*-glycans.** *A*, GII activity toward pNPG or $Glc_1Man_9GlcNAc$ was measured in 125 μg of microsomes from *S. pombe* cells lacking endogenous GIIβ (Δ*GIIβ*) and expressing GIIβ or the same subunit displaying the indicated mutations. The activity of Δ*GIIβ* cells transformed with wild-type GIIβ was taken as 100%. *Error bars* represent S.D. *B*, GIIα ER content was evaluated. Microsomal proteins (250 μg) of *S. pombe* Δ*GIIα*, Δ*GIIβ*, or Δ*GIIβ* expressing exogenous variants of GIIβ were resolved by 8% SDS-PAGE, transferred to a PVDF membrane, and blotted using mouse polyclonal anti-GIIα (1:500) or anti-GIIβ (1:5000) subunit primary antibodies. Goat HRP anti-mouse IgG (1:5000) was used as the secondary antibody. Reactions were detected by chemiluminescence. Because endogenous GIIβ levels are significantly lower than exogenously expressed levels, the GIIβ band was detected in the GIIα mutant (*middle lane*; Δ*GIIα*) only upon overexposing the blot. *C–F*, glycan patterns synthesized by *S. pombe* Δ*GIIβ* mutant cells expressing GIIβ (*C*) or mutated GIIβ versions (*D* and *E*). Endoplasmic reticulum *N*-glycans produced by Δ*GIIβ* cells expressing GIIβ W409A were indistinguishable from those produced by cells expressing GIIβ W409F. The *N*-glycan pattern produced by Δ*GIIβ* cells expressing GIIβ E433Q was indistinguishable from that of the same cells expressing GIIβ Y439F. Quantification of the relative amounts of the di-, mono-, and unglucosylated species in each mutant is shown in *F*. The label of Man_8 species was added to that in Man_9 species to account for unglucosylated glycans.

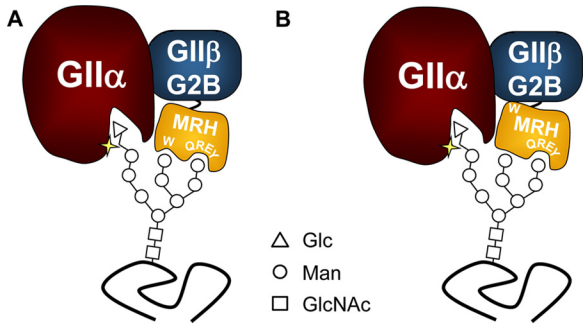

FIGURE 11. **Possible models for the influence of Trp-409 in GII activity.** In *A*, mannose-binding essential residues Gln-384, Arg-414, Glu-433, and Tyr-439 form a pocket that binds arm C of the glycan, whereas residue Trp-409 interacts with arm B. This bidentate interaction allows the glucose-containing arm A to be juxtaposed to the catalytic site of GIIα. In *B*, Trp-409 interacts with other regions of the β-subunit and influences its affinity for *N*-glycans. Note that in both models binding of the C arm of the glycan to the binding pocket of GIIβ MHR domain is required for an efficient presentation of the C arm to the GIIα catalytic subunit. This implies that removal of mannoses by ER mannosidases will reduce binding of the glycan and GII activity as has been shown in the model presented in Ref. 15.

in arm A of the glycan becoming optimally positioned into the catalytic site. Both models indicate that the active site of GIIα must be very close to that of the binding pocket of the MRH domain of GIIβ. In comparison with the other MRH domains, the shorter loops between strands 2 and 3 and strands 4/5 and 6 along with shorter strands 4/5 and 6 (Fig. 5*D*) may allow a close juxtapositioning of the catalytic site with the MRH domain.

Concluding Remarks—In the current study, we have determined the solution structure of the *S. pombe* GIIβ MRH domain, and its function was characterized alone and in the context of the full-length GIIβ subunit. This is the first time that the structure of an MRH domain of an enzyme has been determined. The structure reveals the conserved MRH fold observed in the MPRs (35, 39–42) and OS-9 (7), but in contrast to these proteins, GIIβ MRH domain contains a shallow binding pocket that accommodates only a single mannose residue. In addition, we have identified a conserved residue, Trp-409, that plays an important role in GII glucose trimming activity *in vivo*. Additional structural studies are needed to fully understand how this heterodimeric enzyme interacts with *N*-glycans and thus regulates the quality control of glycoprotein folding in the ER.

Acknowledgments—The BIAcore 3000 instrument was purchased through a grant from the Advancing a Healthier Wisconsin program. Acid α-glucosidase was generously provided by Dr. William Canfield. We thank Drs. J. J. Caramelo, L. Alonso, and G. Paris from the Fundación Instituto Leloir for helpful discussions and advice with GIIβ purification. UDP-[^{14}C]Glc was efficiently synthesized by Susana Raffo. We also thank Dr. Jung-Ja Kim for critical reading of the manuscript.

REFERENCES

1. Castonguay, A. C., Olson, L. J., and Dahms, N. M. (2011) Mannose 6-phosphate receptor homology (MRH) domain-containing lectins in the secretory pathway. *Biochim. Biophys. Acta* **1810,** 815–826
2. Munro, S. (2001) The MRH domain suggests a shared ancestry for the mannose 6-phosphate receptors and other N-glycan-recognising proteins. *Curr. Biol.* **11,** R499–R501
3. Hammond, C., Braakman, I., and Helenius, A. (1994) Role of N-linked oligosaccharide recognition, glucose trimming, and calnexin in glycoprotein folding and quality control. *Proc. Natl. Acad. Sci. U.S.A.* **91,** 913–917
4. D'Alessio, C., Caramelo, J. J., and Parodi, A. J. (2010) UDP-GlC:glycoprotein glucosyltransferase-glucosidase II, the ying-yang of the ER quality control. *Semin. Cell Dev. Biol.* **21,** 491–499
5. Hosokawa, N., Kamiya, Y., Kamiya, D., Kato, K., and Nagata, K. (2009) Human OS-9, a lectin required for glycoprotein endoplasmic reticulum-associated degradation, recognizes mannose-trimmed *N*-glycans. *J. Biol. Chem.* **284,** 17061–17068
6. Quan, E. M., Kamiya, Y., Kamiya, D., Denic, V., Weibezahn, J., Kato, K., and Weissman, J. S. (2008) Defining the glycan destruction signal for endoplasmic reticulum-associated degradation. *Mol. Cell* **32,** 870–877
7. Satoh, T., Chen, Y., Hu, D., Hanashima, S., Yamamoto, K., and Yamaguchi, Y. (2010) Structural basis for oligosaccharide recognition of misfolded glycoproteins by OS-9 in ER-associated degradation. *Mol. Cell* **40,** 905–916
8. Fujimori, T., Kamiya, Y., Nagata, K., Kato, K., and Hosokawa, N. (2013) Endoplasmic reticulum lectin XTP3-B inhibits endoplasmic reticulum-associated degradation of a misfolded α1-antitrypsin variant. *FEBS J.* **280,** 1563–1575
9. Trombetta, E. S., Simons, J. F., and Helenius, A. (1996) Endoplasmic reticulum glucosidase II is composed of a catalytic subunit, conserved from yeast to mammals, and a tightly bound noncatalytic HDEL-containing subunit. *J. Biol. Chem.* **271,** 27509–27516
10. D'Alessio, C., Fernández, F., Trombetta, E. S., and Parodi, A. J. (1999) Genetic evidence for the heterodimeric structure of glucosidase II. The effect of disrupting the subunit-encoding genes on glycoprotein folding. *J. Biol. Chem.* **274,** 25899–25905
11. Grinna, L. S., and Robbins, P. W. (1980) Substrate specificities of rat liver microsomal glucosidases which process glycoproteins. *J. Biol. Chem.* **255,** 2255–2258
12. Totani, K., Ihara, Y., Matsuo, I., and Ito, Y. (2006) Substrate specificity analysis of endoplasmic reticulum glucosidase II using synthetic high mannose-type glycans. *J. Biol. Chem.* **281,** 31502–31508
13. Hu, D., Kamiya, Y., Totani, K., Kamiya, D., Kawasaki, N., Yamaguchi, D., Matsuo, I., Matsumoto, N., Ito, Y., Kato, K., and Yamamoto, K. (2009) Sugar-binding activity of the MRH domain in the ER α-glucosidase II β subunit is important for efficient glucose trimming. *Glycobiology* **19,** 1127–1135
14. Stigliano, I. D., Caramelo, J. J., Labriola, C. A., Parodi, A. J., and D'Alessio, C. (2009) Glucosidase II β subunit modulates N-glycan trimming in fission yeasts and mammals. *Mol. Biol. Cell* **20,** 3974–3984
15. Stigliano, I. D., Alculumbre, S. G., Labriola, C. A., Parodi, A. J., and D'Alessio, C. (2011) Glucosidase II and N-glycan mannose content regulate the half-lives of monoglucosylated species *in vivo*. *Mol. Biol. Cell* **22,** 1810–1823
16. Quinn, R. P., Mahoney, S. J., Wilkinson, B. M., Thornton, D. J., and Stirling, C. J. (2009) A novel role for Gtb1p in glucose trimming of N-linked glycans. *Glycobiology* **19,** 1408–1416
17. Moreno, S., Klar, A., and Nurse, P. (1991) Molecular genetic analysis of fission yeast *Schizosaccharomyces pombe*. *Methods Enzymol.* **194,** 795–823
18. Alfa, C., Fantes, P., Hyams, J., McLeod, M., and Wabrik, E. (1993) *Experiments with Fission Yeast: A Laboratory Manual*, pp. 133–136, Cold Spring Harbor Laboratory Press, Cold Spring Harbor, NY
19. Jannatipour, M., and Rokeach, L. A. (1995) The *Schizosaccharomyces pombe* homologue of the chaperone calnexin is essential for viability. *J. Biol. Chem.* **270,** 4845–4853
20. Matsuyama, A., Arai, R., Yashiroda, Y., Shirai, A., Kamata, A., Sekido, S., Kobayashi, Y., Hashimoto, A., Hamamoto, M., Hiraoka, Y., Horinouchi, S., and Yoshida, M. (2006) ORFeome cloning and global analysis of protein localization in the fission yeast *Schizosaccharomyces pombe*. *Nat. Biotechnol.* **24,** 841–847
21. Wright, A., Dankert, M., and Robbins, P. W. (1965) Evidence for an intermediate stage in the biosynthesis of the *Salmonella* O-antigen. *Proc. Natl. Acad. Sci. U.S.A.* **54,** 235–241
22. Trombetta, S. E., Bosch, M., and Parodi, A. J. (1989) Glucosylation of

glycoproteins by mammalian, plant, fungal, and trypanosomatid protozoa microsomal membranes. *Biochemistry* **28,** 8108–8116
23. Allen, H. J., and Johnson, E. A. (1976) The isolation of lectins on acid-treated agarose. *Carbohydr. Res.* **50,** 121–131
24. Walker, J. M. (2002) *The Protein Protocols Handbook*, 2nd Ed., pp. 803–804, Humana Press Inc., Totowa, NJ
25. Fernández, F. S., Trombetta, S. E., Hellman, U., and Parodi, A. J. (1994) Purification to homogeneity of UDP-glucose:glycoprotein glucosyltransferase from *Schizosaccharomyces pombe* and apparent absence of the enzyme from *Saccharomyces cerevisiae*. *J. Biol. Chem.* **269,** 30701–30706
26. Bohnsack, R. N., Song, X., Olson, L. J., Kudo, M., Gotschall, R. R., Canfield, W. M., Cummings, R. D., Smith, D. F., and Dahms, N. M. (2009) Cation-independent mannose 6-phosphate receptor: a composite of distinct phosphomannosyl binding sites. *J. Biol. Chem.* **284,** 35215–35226
27. Myszka, D. G. (2000) Kinetic, equilibrium, and thermodynamic analysis of macromolecular interactions with BIACORE. *Methods Enzymol.* **323,** 325–340
28. Delaglio, F., Grzesiek, S., Vuister, G. W., Zhu, G., Pfeifer, J., and Bax, A. (1995) NMRPipe: a multidimensional spectral processing system based on UNIX pipes. *J. Biomol. NMR* **6,** 277–293
29. Bartels, C., Xia, T. H., Billeter, M., Güntert, P., and Wüthrich, K. (1995) The program XEASY for computer-supported NMR spectral analysis of biological macromolecules. *J. Biomol. NMR* **6,** 1–10
30. Bartels, C., Billeter, M., Güntert, P., and Wüthrich, K. (1996) Automated sequence-specific NMR assignments of homologous proteins using the program GARANT. *J. Biomol. NMR* **7,** 207–213
31. Shen, Y., Delaglio, F., Cornilescu, G., and Bax, A. (2009) TALOS+: a hybrid method for predicting protein backbone torsion angles from NMR chemical shifts. *J. Biomol. NMR* **44,** 213–223
32. Herrmann, T., Güntert, P., and Wüthrich, K. (2002) Protein NMR structure determination with automated NOE assignment using the new software CANDID and the torsion angle dynamics algorithm DYANA. *J. Mol. Biol.* **319,** 209–227
33. Schwieters, C. D., Kuszewski, J. J., Tjandra, N., and Clore, G. M. (2003) The Xplor-NIH NMR molecular structure determination package. *J. Magn. Reson.* **160,** 65–73
34. Linge, J. P., Williams, M. A., Spronk, C. A., Bonvin, A. M., and Nilges, M. (2003) Refinement of protein structures in explicit solvent. *Proteins* **50,** 496–506
35. Olson, L. J., Peterson, F. C., Castonguay, A., Bohnsack, R. N., Kudo, M., Gotschall, R. R., Canfield, W. M., Volkman, B. F., and Dahms, N. M. (2010) Structural basis for recognition of phosphodiester-containing lysosomal enzymes by the cation-independent mannose 6-phosphate receptor. *Proc. Natl. Acad. Sci. U.S.A.* **107,** 12493–12498
36. Chavez, C. A., Bohnsack, R. N., Kudo, M., Gotschall, R. R., Canfield, W. M., and Dahms, N. M. (2007) Domain 5 of the cation-independent mannose 6-phosphate receptor preferentially binds phosphodiesters (mannose 6-phosphate N-acetylglucosamine ester). *Biochemistry* **46,** 12604–12617
37. Kim, J. J., Olson, L. J., and Dahms, N. M. (2009) Carbohydrate recognition by the mannose-6-phosphate receptors. *Curr. Opin. Struct. Biol.* **19,** 534–542
38. Watanabe, T., Totani, K., Matsuo, I., Maruyama, J., Kitamoto, K., and Ito, Y. (2009) Genetic analysis of glucosidase II β-subunit in trimming of high-mannose-type glycans. *Glycobiology* **19,** 834–840
39. Olson, L. J., Yammani, R. D., Dahms, N. M., and Kim, J. J. (2004) Structure of uPAR, plasminogen, and sugar-binding sites of the 300 kDa mannose 6-phosphate receptor. *EMBO J.* **23,** 2019–2028
40. Usón, I., Schmidt, B., von Bülow, R., Grimme, S., von Figura, K., Dauter, M., Rajashankar, K. R., Dauter, Z., and Sheldrick, G. M. (2003) Locating the anomalous scatterer substructures in halide and sulfur phasing. *Acta Crystallogr. D Biol. Crystallogr.* **59,** 57–66
41. Brown, J., Delaine, C., Zaccheo, O. J., Siebold, C., Gilbert, R. J., van Boxel, G., Denley, A., Wallace, J. C., Hassan, A. B., Forbes, B. E., and Jones, E. Y. (2008) Structure and functional analysis of the IGF-II/IGF2R interaction. *EMBO J.* **27,** 265–276
42. Roberts, D. L., Weix, D. J., Dahms, N. M., and Kim, J.-J. (1998) Molecular basis of lysosomal enzyme recognition: three-dimensional structure of the cation-dependent mannose 6-phosphate receptor. *Cell* **93,** 639–648
43. Mikami, K., Yamaguchi, D., Tateno, H., Hu, D., Qin, S. Y., Kawasaki, N., Yamada, M., Matsumoto, N., Hirabayashi, J., Ito, Y., and Yamamoto, K. (2010) The sugar-binding ability of human OS-9 and its involvement in ER-associated degradation. *Glycobiology* **20,** 310–321
44. Totani, K., Ihara, Y., Matsuo, I., and Ito, Y. (2008) Effects of macromolecular crowding on glycoprotein processing enzymes. *J. Am. Chem. Soc.* **130,** 2101–2107
45. Kamiya, Y., Satoh, T., and Kato, K. (2012) Molecular and structural basis for N-glycan-dependent determination of glycoprotein fates in cells. *Biochim. Biophys. Acta* **1820,** 1327–1337
46. Fernández, F., D'Alessio, C., Fanchiotti, S., and Parodi, A. J. (1998) A misfolded protein conformation is not a sufficient condition for *in vivo* glucosylation by the UDP-Glc:glycoprotein glucosyltransferase. *EMBO J.* **17,** 5877–5886
47. Olson, L. J., Dahms, N. M., and Kim, J. J. (2004) The N-terminal carbohydrate recognition site of the cation-independent mannose 6-phosphate receptor. *J. Biol. Chem.* **279,** 34000–34009
48. Woods, R. J., Pathiaseril, A., Wormald, M. R., Edge, C. J., and Dwek, R. A. (1998) The high degree of internal flexibility observed for an oligomannose oligosaccharide does not alter the overall topology of the molecule. *Eur. J. Biochem.* **258,** 372–386
49. Kumari, M., Balaji, P. V., and Sunoj, R. B. (2011) Quantification of binding affinities of essential sugars with a tryptophan analogue and the ubiquitous role of C–H···π interactions. *Phys. Chem. Chem. Phys.* **13,** 6517–6530
50. Stenmark, P., Dupuy, J., Imamura, A., Kiso, M., and Stevens, R. C. (2008) Crystal structure of botulinum neurotoxin type A in complex with the cell surface co-receptor GT1b-insight into the toxin-neuron interaction. *PLoS Pathog.* **4,** e1000129
51. Schallus, T., Jaeckh, C., Fehér, K., Palma, A. S., Liu, Y., Simpson, J. C., Mackeen, M., Stier, G., Gibson, T. J., Feizi, T., Pieler, T., and Muhle-Goll, C. (2008) Malectin: a novel carbohydrate-binding protein of the endoplasmic reticulum and a candidate player in the early steps of protein N-glycosylation. *Mol. Biol. Cell* **19,** 3404–3414
52. Hancock, M. K., Yammani, R. D., and Dahms, N. M. (2002) Localization of the carbohydrate recognition sites of the insulin-like growth factor II/mannose 6-phosphate receptor to domains 3 and 9 of the extracytoplasmic region. *J. Biol. Chem.* **277,** 47205–47212
53. Schrag, J. D., Bergeron, J. J., Li, Y., Borisova, S., Hahn, M., Thomas, D. Y., and Cygler, M. (2001) The structure of calnexin, an ER chaperone involved in quality control of protein folding. *Mol. Cell* **8,** 633–644
54. DeLano, W. L. (2002) *The PyMOL Molecular Graphics System*, Schrödinger, LLC, New York

Structure of the Lectin Mannose 6-Phosphate Receptor Homology (MRH) Domain of Glucosidase II, an Enzyme That Regulates Glycoprotein Folding Quality Control in the Endoplasmic Reticulum

Linda J. Olson, Ramiro Orsi, Solana G. Alculumbre, Francis C. Peterson, Ivan D. Stigliano, Armando J. Parodi, Cecilia D'Alessio and Nancy M. Dahms

J. Biol. Chem. 2013, 288:16460-16475.
doi: 10.1074/jbc.M113.450239 originally published online April 22, 2013
